1 **The blast effector Pwl2 is a virulence factor that modifies the cellular localisation of host protein**
2 **HIPP43 to suppress immunity.**
3

Vincent Were[1], Xia Yan[1], Andrew J. Foster[1], Jan Sklenar[1], Thorsten Langner[1], Adam Bentham[1], Rafał Zdrzałek[2], Lauren Ryder[1], Davies Kaimenyi[1], Diana Gomez De La Cruz[1], Amber Gentle[1], Yohan Petit-Houdenot[4], Alice Bisola Eseola[1], Matthew Smoker[1], Mark Jave Bautista[1], Weibin Ma[1], Jiorgos Kourelis[1], Dan Maclean[1], Mark J. Banfield[2], Sophien Kamoun[1], Frank L.H. Menke[1], Matthew J. Moscou[1,3] and Nicholas J. Talbot[1] *

[1] The Sainsbury Laboratory, University of East Anglia, Norwich Research Park, Norwich, NR4 7UH, United Kingdom.
[2] Department of Biochemistry and Metabolism, John Innes Centre, Norwich Research Park, Norwich, NR4 7UH, United Kingdom.
[3] USDA-ARS Cereal Disease Laboratory, University of Minnesota, 1551 Lindig Street, Saint Paul, Minnesota, 55108 USA.
[4] Université Paris-Saclay, INRAE, UR BIOGER, 91120, Palaiseau, France.

[*]Corresponding author: Nicholas J. Talbot (Nick.Talbot@tsl.ac.uk)

ORCID IDs

Vincent Were:	0000-0002-9885-4877
Xia Yan:	0000-0003-4509-0137
Andrew J. Foster:	0000-0002-8459-7590
Jan Sklenar:	0000-0003-1858-2574
Thorsten Langner:	0000-0002-3401-8888
Adam R. Bentham:	0000-0001-5906-0962
Rafał Zdrzałek:	0000-0003-3669-924X
Lauren Ryder:	0000-0003-0370-5746
Davies Kaimenyi:	0000-0002-6320-3740
Diana Gómez De La Cruz:	0000-0001-6683-9245
Amber Gentle:	0009-0006-1944-4754
Yohann Petit-Houdenot:	0000-0003-4806-8349
Alice Bisola Eseola:	0000-0001-5698-8204
Mark Jave Bautista:	0000-0002-6016-5953
Weibin Ma:	0000-0002-0516-2151
Jiorgos Kourelis:	0000-0002-9007-1333
Dan MacLean:	0000-0003-1032-0887
Mark J. Banfield:	0000-0001-8921-3835
Sophien Kamoun:	0000-0002-0290-0315
Frank L.H.Menke:	0000-0003-2490-4824
Matthew J. Moscou:	0000-0003-2098-6818
Nicholas J Talbot:	0000-0001-6434-7757

Abstract

The rice blast fungus *Magnaporthe oryzae* secretes a battery of effector proteins during host infection to suppress plant immunity and promote disease. Among these effectors, the MAX effector-Pwl2 was first identified as a host specificity determinant for infection of weeping lovegrass (*Eragrostis curvula*). However, its biological activity has remained unknown. Here we show that the *PWL2* gene is ubiquitous in all host-limited forms of *M. oryzae* and has undergone substantial copy number expansion indicating that it is a core effector of the blast fungus. We used CRISPR/Cas9-mediated gene editing to delete all three copies of *PWL2* and generate a *pwl2* null mutant in *M. oryzae* strain Guy11. This resulted in gain-of-virulence towards weeping lovegrass, but a reduction in the severity of disease symptoms on rice. To further investigate the virulence mechanism of Pwl2, we showed that transgenic rice and barley lines constitutively expressing *PWL2* display suppression of reactive oxygen species generation and increased susceptibility to infection by *M. oryzae*. Also, we identify the barley and rice heavy metal-binding isoprenylated protein HIPP43 as a target of the Pwl2 effector. Transgenic lines overexpressing HIPP43 exhibit attenuated defense responses and increased susceptibility to blast infection, consistent with the hypothesis that Pwl2 binds HIPP43 to modulate immunity. This binding is coupled to changes in cellular localisation of these proteins. Taken together, our results provide evidence that Pwl2 is a virulence factor in *M. oryzae* that acts by suppressing host immunity through binding and re-localising HIPP43.

Introduction

Plant pathogens secrete virulence proteins called effectors during infection to suppress the plant immune system and facilitate invasion of host tissue. This process, called effector-triggered susceptibility, enables pathogens to manipulate plant metabolic processes, overcome plant immunity and successfully colonise host plants (1). Fungal pathogens, such as the devastating blast fungus *Magnaporthe oryzae* (which destroys enough rice to feed 60 million people every year) deploy an extensive battery of effectors, with more than 500 identified to date (2, 3), but very few are functionally characterised (4). However, effectors are also recognised by plant intracellular nucleotide-binding leucine rich repeat (NLR) immune receptors to activate disease resistance. For example, in rice, the paired NLRs RGA5/RGA4, Pik-1/Pik-2, and Piks-1/Piks-2 confer resistance to *M. oryzae* strains that secrete AVR1-CO39/AVR-Pia, AVR-Pik or AVR-Mgk1 effectors, respectively (5-9). Each of these proteins are members of the *Magnaporthe* Avrs and ToxB-like (MAX) effector family that are sequence unrelated, but structurally conserved (10), and are overrepresented among effectors recognised by rice NLR immune receptors (6, 7, 11, 12). Pwl2 was first identified as a host specificity determinant that controls pathogenicity towards weeping lovegrass (*Eragrostis curvula*), a widely grown forage grass and was recently shown to be recognised in barley by the Mla3 immune receptor (13, 14) While *PWL2* has been widely studied and used as an important tool to understand effector secretion and delivery, the molecular mechanisms by which Pwl2 interacts with the host have remained unknown, with little research into the virulence function of this effector.

A companion paper Zdrzałek *et al* (15) identifies Pwl2 as a MAX effector, and recent studies of MAX-effector perception by NLRs have identified host small heavy metal-associated (sHMA) domain containing proteins to be the likely targets of several of these effectors. Small HMA proteins are highly expanded across plant species with putative functions ranging from heavy metal detoxification, to potential metallochaperones and other yet to be characterised functions (16-18). These proteins can be broadly separated into two families, heavy metal-associated plant proteins (HPPs), and heavy-metal associated isoprenylated plant proteins (HIPPs), of which the latter possess a C-terminal isoprenylation motif (CaaX, where ‘a’ represents an aliphatic residue and ‘X’ is any amino acid) important for anchoring to

membranes (19). The rice sHMA protein Pi21 is a disease susceptibility factor, with rice lines expressing this protein exhibiting delayed defence responses to rice blast (19, 20). This has led to the use of loss-of-function alleles of *pi21*, as a recessive form of rice blast resistance in breeding programs (20). Furthermore, differences in host sHMA protein repertoires have been linked to host-specific adaptive evolution of the APikL2 effector family, while studies of AVR-Pik and its target OsHIPP20 suggests that effector binding may stabilize the host protein (21, 22). Importantly, sHMA protein domains have also been found integrated as non-canonical immune sensory domains in some NLR proteins, such as the rice Pik-1/2 and Pia (RGA5/4) receptors, and are essential for recognition of their cognate *M. oryzae* effectors (6, 8, 9, 11). The integration of sHMA proteins into immune receptors further underlines the relevance of sHMA proteins in pathogen virulence. However, the exact function of sHMA proteins in plants and their link to disease susceptibility in plant-pathogen interactions is still poorly understood, obscuring the specific function of MAX effectors that target these proteins.

In this study, we investigate the biological function of *PWL2* and its role in fungal pathogenesis. We were motivated to understand how a ubiquitous effector like Pwl2 functions during a susceptible interaction between *M. oryzae* and its host. We demonstrate that the *PWL2* gene is ubiquitous across *M. oryzae* lineages and has undergone significant gene duplication and expansion in copy number, with many rice blast isolates possessing 3-5 copies, making its functional analysis challenging. Using CRISPR-Cas9 gene editing, we generated a *pwl2* null mutant and verified the role of Pwl2 as a host specificity determinant towards weeping lovegrass and barley lines containing *Mla3*. We constructed transgenic rice and barley lines constitutively expressing *PWL2* and show that Pwl2 suppresses PAMP-triggered immunity through attenuation of the ROS burst, resulting in increased susceptibility to rice blast. Finally, we reveal that Pwl2 targets the sHMA protein HIPP43 in both rice and barley and show that transgenic plants overexpressing HIPP43 have reduced immune responses. We also show that Pwl2 co-localizes and alters sub-cellular localisation of HIPP43 in *Nicotiana benthamiana*. Taken together, our study provides evidence that Pwl2 plays a role in defence suppression by binding and re-localising HIPP43 to facilitate colonization of plant tissue by the blast fungus.

Results

Pwl2 is an *in-planta* effector, expressed during infection and localizes to the BIC.

The *PWL2* gene is specifically expressed during the biotrophic phase of infection, peaking in expression at 36 - 48 hours post-infection (hpi) (3) (**Fig. S1*A* and *B***). The Pwl2 effector localises in the biotrophic interfacial complex (BIC) and is clearly visible as a single bright punctum, initially at the tip of an invasive hypha and then adjacent to the bulbous, branched hyphae as they develop (**Fig. 1*A* and *B*).** The BIC is a plant membrane-rich structure and the predicted site of effector delivery (23-25), although experiments to date have not precluded that the BIC could be a site of effector sequestration by the host. To investigate Pwl2 secretion at the BIC during infection, we generated a single *M. oryzae* strain expressing two BIC-localised effectors Pwl2-mRFP and Bas1-GFP and visualised their localisation during infection of leaf sheath tissue of the susceptible rice cultivar Moukoto. The two effectors were observed as small punctate signals within the same BIC (**Fig. 1*A* and *C***). By contrast, when two different *M. oryzae* strains, Ina168 and Guy11, expressing Pwl2-GFP and Pwl2-mRFP respectively were used to simultaneously infect rice tissue, we observed that the BIC formed by each individual invasive hypha harboured exclusively either Pwl2-GFP or Pwl2-mRFP but never both signals (**Fig. 1*B* and *D*).** This suggests that the Pwl2 effector is secreted from the BIC into host cells, especially when considered with previous reports showing the BIC to be the site of unconventional fungal secretion and clathrin-mediated endocytosis (24).

PWL2 is ubiquitous in isolates of *M. oryzae.*

The *PWL2* effector belongs to a wider gene family (13, 26), but conservation of the *PWL* family in the global rice blast population, and among different host-limited forms of *M. oryzae*, is not fully known. Therefore, we investigated *PWL* gene family conservation in publicly available genome sequences, including isolates that infect *Oryza sativa* (rice), *Eleusine* spp. (finger millet), *Hordeum vulgare* (barley), *Setaria* spp. (foxtail millet), *Triticum aestivum* (wheat), *Lolium* spp. (rye grass), *Brachiaria* spp. (signal grass), *Panicum repens* (torpedo grass) and *Eragrostis* spp (weeping lovegrass) (27-30). We also included two close relatives of *M. oryzae* that infect crabgrass (*Digitaria sanguinalis*) and pearl millet (*Pennisetum* spp.). We used Pwl1 (BAH22184.1), Pwl2 (QNS36448.1), Pwl3 (AAA80240.1) and Pwl4 (AAA80241.1) protein sequences to query for the presence or absence of each protein-encoding gene. We observed that *PWL1* is present in group EC-1I (31) of *Eleusine*-infecting isolates, one *Eragrostis*-infecting isolate and some *Oryza*-infecting isolates but absent in all the other host-specific lineages (**Fig. 1*F* and S2*B*)**. Similarly, *PWL3* is found in most *Oryza*-infecting isolates, but almost completely lost in the other lineages, except for some *Setaria*, *Lolium*, and *Eleusine*-infecting isolates. *PWL4* is present in *Eleusine*, *Lolium* and *Triticum*-infecting isolates, but almost completely lost in *Oryza*-infecting isolates. We however found one *Digitaria*-infecting isolate that carry *PWL4* (**Fig. S2*B***). In contrast to all other *PWL* family members, *PWL2* is found in all host-limited forms of *M. oryzae* and related *Magnaporthe* species (**Fig. 1*E* and S2*B***). We conclude that Pwl2 is a core effector of the blast fungus.

Having determined Pwl2 is ubiquitous in isolates of *M. oryzae*, we next sought to determine how polymorphic the effector is, in different host-limited forms of *M. oryzae*. Apart from the *pwl2-2* variant that contains a single Asp-90-Asn substitution (13, 14), we found 14 new variants of Pwl2 that can be renamed Pwl2-3 to Pwl2-14. Majority of the polymorphic residues occurred at positions His87 to Ser92 (**Fig. S2*A***). In comparison, we identified 2 variants of Pwl1 (renamed Pwl1-2 and Pwl1-3), 4 variants of Pwl3 and 1 variant of Pwl4 (**Fig. S3*A*, *B* and *C***). From this analysis, we conclude that Pwl2 is highly polymorphic compared to other members in the family. We next tested the ability of *PWL2* variant alleles to be recognised on

known resistant hosts. A subset of the isolates carrying variants of *PWL2* BTJP4-16 (*pwl2-3)*, JUM1 (*pwl2-2*), BN0293 (variant *Pwl2*), BF5 (variant *Pwl2*), VO107 (variant *Pwl2*), and PM1 (variant *Pwl2*) were used to infect barley lines that carry *Mla3* or weeping lovegrass. Some of the variants were identified in same background isolate carrying *PWL1,* one or multiple copies of *PWL2*, and it was not possible functionally characterise them using infection assays. We found BTJP4-16 (*pwl2-3)*, JUM1 (*pwl2-2*) and BN0293 to be virulent on these hosts, providing evidence that these alleles are non-functional (**Fig. S2*C-D***). Isolates VO107, BF5 and PM1 did not produce blast disease lesions in the presence of *Mla3* suggesting that alleles present in these isolates were either recognised by the host, or the *M. oryzae* isolates carry other effectors recognised by additional R-genes contained in barley cv. Baronesse or weeping lovegrass. (**Fig. S2*E***).

Pwl2 allelic variability affecting host specificity is not associated with the MAX effector fold.

The majority of *Oryza*-, *Lolium*- and *Triticum*-infecting isolates of *M. oryzae* analysed have *PWL2* or the variant *pwl2-2* allele, which is associated with gain of virulence to *E. curvula* and *Mla3* (**Fig. S1*C*)** (13, 14). Our analyses of the presence of *PWL2* in *Lolium* and *Triticum*-infecting isolates from the pandemic wheat blast lineage (32) identified an allele of *PWL2,* designated *pwl2-3*, with several polymorphisms in the core effector fold: Glu-89-Gln, Lys-91-Gln and Ser-92-Ile (**Fig. 1*E*, S1*D* and S2*A*)**. Interestingly, *pwl2-3* was also identified from *Digitaria* and *Pennisetum spp*-infecting isolates of *Magnaporthe* (**Fig. 1*F*, S2*A* and *B*)**. In an accompanying paper by Zdrzalek *et al* (15) Pwl2 has been structurally verified as a predicted MAX effector, with a core β-sandwich fold formed of two antiparallel β-sheets, as well as a single α-helix, C-terminal to the β-sandwich fold. We therefore mapped a subset of the identified polymorphic residues of Pwl2 including *pwl2-3* to the effector crystal structure. All polymorphisms between *pwl2* alleles were found to reside in the C-terminal α-helix, a distinct region from the core MAX-fold (**Fig. 1*E*)**. This suggests that the interface used to bind Pwl2 by the immune receptors present in resistant barley (Mla3) and weeping love grass, unlikely involves the MAX-fold.

***PWL2* occurs in high copy number in *M. oryzae* field isolates.**

The *M. oryzae* reference genome assembly (strain 70-15) has two copies of *PWL2* on chromosomes 3 and 6, annotated as MGG_04301 and MGG_13683, respectively. We observed, however, that *PWL2* copy number varies significantly in different *M. oryzae* isolates. Southern blot hybridization (**Fig. S4**), and analysis of long-read assembled genomes of the *M. oryzae* rice pathogenic strain Guy11 identified three copies of *PWL2*. A duplication of *PWL2* is present on a single contig in the Guy11 genome, whilst the third copy involves a translocation resulting in a distinct *PWL2* allele in a separate contig (**Fig. 2*A*)**. We observed that the *PWL2* loci were associated with the occurrence of *MGR583*, *POT2* and *MAGGY* transposable elements, suggesting a possible involvement in genome translocation. To further assess *PWL2* copy number in *M. oryzae* isolates, we employed a k-mer analysis approach to determine copy number variation of *PWL2* in *M. oryzae* genomes (n = 286). Strikingly, *PWL2* copy number was high in many *M. oryzae* strains, with one isolate showing 8 copies (**Fig. 2*B*)**. We conclude that *PWL2* is ubiquitous in *Magnaporthe* and has expanded in copy number both in *M. oryzae* and its sister species *M. grisea.*

171 ***Δpwl2* mutants show altered host range and are reduced in ability to cause rice blast**
172 **disease.**

173 Having determined the copy number variation of *PWL2* in *M. oryzae*, we used a CRISPR/Cas9
174 genome editing approach to simultaneously delete the three copies of *PWL2* found in Guy11
175 (33). We designed a sgRNA to target *PWL2* and introduced a hygromycin phosphotransferase-
176 encoding gene cassette (*HPH*) (**Fig. 3*A***). To identify *Δpwl2* null mutants, transformants were
177 analysed by PCR using primers designed to amplify the *PWL2* coding sequence. Transformants
178 with ectopic integrations or where not all copies of *PWL2* were deleted, gave a predicted
179 amplicon size of 645 bp, consistent with untransformed Guy11. By contrast, in null mutants,
180 we amplified a larger amplicon of 1.5 kb, consistent with introgression of the hygromycin
181 resistance cassette into all three copies of *PWL2* (**Fig. 3*A***). Four putative transformants were
182 then selected for whole genome sequencing. Raw reads were aligned to the *M. oryzae* reference
183 genome using samtools v.15, before converting into BAM files and visualised using IGV
184 viewer. No reads mapping to the *PWL2* locus were identified in mutants T6 and T12 whereas
185 fewer reads mapped to the same locus from sequenced T5 and T4 (**Fig. S5**). Regions upstream
186 and downstream of the *PWL2* coding sequence were 100 % identical in both mutants and
187 reference genomes. This confirmed that T6 and T12 are *Δpwl2* gene deletion transformants and
188 they were therefore selected for further analysis. We reasoned that *M. oryzae Δpwl2* deletion
189 mutants would gain virulence on weeping lovegrass (13, 26) and the barley cultivar Baronesse
190 carrying *Mla3* cultivars of barley. The *Δpwl2* deletion transformants T5, T6 and T12 and
191 Guy11 were therefore used to inoculate weeping lovegrass seedlings. We observed that the
192 *Δpwl2* mutants T6, T5 and T12 showed gain of virulence and symptoms of infection which
193 were identical to those exhibited by a virulent G17 isolate that lacks *PWL2* (**Fig. 3*B***). We
194 conclude that T5, T6 and T12 are loss of recognition mutants of *PWL2,* and we can be confident
195 that T6 and T12 have complete deletion of all three copies of the gene.
196 We next tested whether Pwl2 has a virulence function during a compatible interaction between
197 the blast fungus and its host. The *Δpwl2* mutant T6 was infected on the susceptible rice cultivar
198 CO39, susceptible barley lines Nigrate, Siri (*Mla8*), Golden Promise (*Mla8*), and resistant
199 cultivar Baronesse (*Mla3*). The *Δpwl2* mutants showed a small but reproducible reduction in
200 virulence on CO39 compared to wildtype Guy11, based on observed disease lesion size (**Fig.**
201 **3*C* and *E***). Additionally, *Δpwl2* produced statistically smaller lesion sizes on barley lines Siri
202 and Golden Promise (**Fig. 3*D* and *F***). We conclude that *PWL2* contributes to the ability of *M.*
203 *oryzae* to cause blast disease.

204 **Pwl2 suppresses host immunity.**

205 Having determined that the Pwl2 effector contributes to virulence, we aimed to gain insight
206 into its biological function during host cell colonisation. We generated stable transgenic barley
207 (Golden Promise) and rice (Kitaake) lines expressing *PWL2-YFP* (without its signal peptide)
208 under control of the CaMV35S promoter. Transgenic lines expressing cytoplasmic YFP were
209 used as controls. Transgenic plants, expressing Pwl2 and free YFP did not show any adverse
210 growth or fitness phenotypes (**Fig. 4*A***). We first assayed *PWL2-YFP* transgenics for their
211 response to two elicitors of PAMP-triggered immunity, flg22 and chitin. Rice and barley
212 perceive flg22 through the pattern recognition receptor FLS2 and perceive chitin through
213 CEBiP and CERK1 leading to immune response for example production of reactive oxygen
214 species (ROS) (34, 35). We observed that Pwl2 expression abolished chitin and flg22-induced
215 ROS generation (**Fig. 4*B and C***). Pwl2 therefore contributes to virulence by suppressing
216 PAMP-triggered immunity during compatible interactions. To investigate the effect of elevated
217 Pwl2 effector expression on blast infections, we infected barley plants expressing Pwl2 with

218 *M. oryzae* Guy11. Pwl2-expressing lines were significantly more susceptible and developed
219 blast disease symptoms earlier (2-3 dpi) compared to infection of isogenic Golden Promise
220 plants (**Fig. 4*D and E***). We conclude that Pwl2 is a modulator of plant immunity.

221 **Pwl2 binds to the heavy metal binding domain isoprenylated protein, HIPP43.**

222 To determine the likely target of Pwl2, transgenic barley and rice plants expressing Pwl2-YFP
223 were used for protein extraction before performing anti-YFP co-immunoprecipitation coupled
224 to mass spectrometry (IP-MS). This revealed a total of 791 proteins after spectral search in the
225 *H. vulgare* (barley, cv Morex version 3) proteome database. We identified a total of 282
226 frequently occurring proteins in the biological replicates containing Pwl2, that were not
227 identified in the six free-YFP control samples. To avoid focusing on false positives in the form
228 of sticky and abundant proteins, fold-changes were calculated by first determining the average
229 number of peptides per protein candidate, before estimating $\log_2$ fold change compared to the
230 control experiment. We further filtered for proteins that produced at least two peptide hits in
231 more than half of replicates ($\geq$4/8 biological replicates). A total of 52 proteins met this criterion
232 and were considered as enriched in samples compared to controls and were therefore selected
233 for further analysis. Furthermore, because Pwl2 attenuates the ROS-burst in barley transgenics
234 lines, we focused initially on protein candidates previously reported to have roles in plant
235 immunity or ROS generation (**Fig. 4*F***). These were selected for one-to-one interactions using
236 a yeast-two-hybrid (Y2H) assay by co-transforming constructs expressing Pwl2 and Putative
237 Pwl2 Interacting Proteins (PPIPs) identified by IP-MS (**Fig. 4*F* and Fig. S6)**. Pwl2 showed
238 strong binding to PPIP4 (**Fig. 4*G* and *H***). We named this protein HvHIPP43, for *Hordeum*
239 *vulgare* heavy metal binding domain containing isoprenylated plant protein 43 based on
240 homology to *Os*HIPP43 defined in a companion paper by Zdrzalek *et al* (15). To validate the
241 interaction between Pwl2 and HIPP43, we carried out co-immunoprecipitation (co-IP) analysis
242 in *N. benthamiana* and could detect HvHIPP43 interacting with Pwl2-YFP (**Fig. 4*H***). Having
243 determined that Pwl2 binds to HvHIPP43, we investigated the *PWL* gene family-encoded
244 proteins Pwl1, Pwl3, Pwl4 and pwl2-3 variant and showed that they were all able to bind
245 HvHIPP43 in Y2H assays, confirming that Pwl2 belongs to an effector family that binds to a
246 host sHMA protein (**Fig. 4*I***).

247 **Pwl2 interacts with HIPP43 orthologs from other grass species.**

248 HIPPs are expanded in plant genomes and to test whether HIPP43 has orthologs in other grass
249 species, we generated a maximum likelihood phylogenetic tree of HMA domains from diverse
250 grasses with high quality genomes and annotations. We found that the HIPP43 family formed
251 a distinct clade which included orthologs from rice (*O. sativa)*, wheat (*T. aestivum*), wild wheat
252 (*Haynalidia villosa*), foxtail millet (*S. italica*), weeping lovegrass (*E. curvula*), Sorghum
253 (*Sorghum bicolor*), *Oropetium thomaeum*, *Zea mays* and *Brachypodium distachyon* (**Figure**
254 **S7 and S8**). Furthermore, we could identify copy number variation ranging from one to five
255 copies in grasses, with barley and wheat (i.e. Triticeae lineage) having three paralogs of
256 HIPP43, one per haploid genome. We followed this by confirming that, Pwl2 interacts with
257 HvHIPP43 orthologs from *Triticum* (*Taes*HIPP43), *Setaria* (*Siti*HIPP43), and *Eragrostis*
258 (*Ec*HIPP43), in Y2H assays (**Fig. 4*J***). Binding of Pwl2 to rice *Os*HIPP43 was verified by in
259 vitro biochemistry and a structure of the complex obtained from *X*-ray crystallography (see
260 companion paper by Zdrzalek *et al* (15). We also analyzed the transcriptional profile of
261 *Os*HIPP43 during infection of Guy11 on a susceptible rice line CO39 from dataset available
262 from Yan *et al* (3). Interesting we found that, *Os*HIPP43 expression was up regulated during
263 plant infection, suggesting it might play an important role in plant immune response.

264 **Overexpression of HIPP43 suppresses PAMP-induced ROS in transgenic barley.**

265 To investigate the biological relevance of the interaction between Pwl2 and HIPP43, we
266 generated barley transgenic lines overexpressing HIPP43. These transgenic lines were
267 challenged with two elicitors of PAMP-triggered immunity, flg22 and chitin. Strikingly, we
268 observed that the chitin and flg22-induced ROS burst was abolished in plants expressing
269 HIPP43 compared to wild type and plants expressing free YFP (**Fig. 5 *A, B, C* and *D*)**.
270 Similarly, when we challenged transgenic barley plants expressing HIPP43 with *M. oryzae*, we
271 observed increased susceptibility compared to the wildtype Golden Promise with disease
272 lesions appearing earlier than in wild type plants. This observation is consistent with earlier
273 results showing attenuated ROS burst in plants expressing Pwl2-YFP (**Fig. 5*E* and *F*)**.

274 **Isoprenylation motif is required for HIPP43 plasmodesmata localization.**

275 So far, there is no direct evidence for the involvement of HIPP proteins in host immunity and
276 regulation of ROS so we reasoned that HIPP43 might bind to another host protein following
277 interaction with Pwl2. HIPP43 possesses an isoprenylation motif at its C-terminus (**Figure
278 S9*A***), and we performed live cell imaging of mCherry and YFP-tagged HIPP43 (at the N or C
279 terminus, respectively), following transient expression in *N. benthamiana* to determine the
280 localisation of the protein. We also tested localisation of HIPP43 without its predicted
281 isoprenylation motif. When tagged at the N-terminus, HIPP43 mainly localises to puncta at the
282 plasma membrane that co-localise with callose staining (aniline blue) consistent with these
283 being sites of plasmodesmata (PD) (**Fig. 5*G* and *H*)**. However, without its isoprenylation
284 motif, PD localisation was abolished, and we observed accumulation in the nucleoplasm and
285 plasma membrane (**Fig. S9*B*)**. When tagged at its C-terminus (HIPP43-YFP), HIPP43 mainly
286 localises to PD, cytoplasm, plasma membrane and chloroplasts (**Fig. S9*C*)**.

287 **Pwl2 stabilises and alters plasmodesmata localization of HIPP43.**

288 When we co-expressed YFP-Pwl2 with mCherry-HIPP43, we observed co-localisation in the
289 cytoplasm with the appearance of cytoplasmic mobile bodies approximately 2 µm in diameter,
290 likely to be very large vesicles or P-bodies (**Fig. 5*I*)**. In some cases, we also observed larger
291 cytoplasmic mobile bodies ranging from 2-4 µm in diameter (**Fig. 5*I*)**. We quantified the
292 number of times HIPP43 signal was observed at PD when co-expressed with free-YFP, AVR-
293 PikE and the effector Mep3 (3) as controls. We observed that co-localisation of YFP-Pwl2 and
294 mCherry-HIPP43 as cytoplasmic vesicles compromised PD localisation (**Fig. 5*I* and *J*)**.. In
295 addition, localization of HIPP43 in large cytoplasmic mobile bodies was not observed when
296 we co-localised HIPP43 with empty vector controls expressing YFP (**Fig. 5*K* and *L*)** or two
297 other MAX-fold effectors, AVR-PikE (**Fig. 5*M* and *N*)** and MEP3 (**Fig. S10*E* and *F*),** as it
298 remained localised at PDs. Moreover, the intensity of mCherry-HIPP43 fluorescence was
299 higher when co-expressed with Pwl2 compared to when expressed in the absence of Pwl2, or
300 when co-expressed with free YFP, AVR-PikE or MEP3 **(Fig. 5*I* and Fig. S10*D*)**. When
301 considered together, these results suggest that Pwl2 binds to HIPP43, potentially stabilising the
302 protein and altering its cellular location away from plasmodesmata.

Discussion

The Pwl2 effector was first identified as a host specificity determinant for infection of the forage grass species weeping lovegrass (13, 26). Its initial identification provided evidence that host range in plant pathogenic fungi was conditioned in a similar way to cultivar specificity in a gene-for-gene manner, involving dominant pathogen genes recognised by the products of cognate disease resistance genes (26). Furthermore, Pwl2 was found to belong to an expanded gene family, suggesting an important function in pathogenicity and fitness (26). However, in the following two decades, the function of Pwl2 has remained elusive despite its extensive use as a marker in cell biological studies for investigating effector regulation, secretion and delivery during plant infection (23-25).

In this study, we set out to explore the function of Pwl2 and investigate why it is such a ubiquitous effector in *Magnaporthe oryzae*. We found that the *PWL2* gene is present across all rice blast lineages, and in all publicly available genome sequences of *M. oryzae*, including each of its host-limited forms and even in sister species infecting crabgrass and pearl millet. The observation that *PWL2* and the wider *PWL* family genes have been maintained in the global blast population and occurrence of effector variants or loss-of-recognition alleles associated with certain host-adapted lineages, suggests that Pwl2 and members of this family serve an important function in pathogenesis. Furthermore, *PWL2* is present at high copy number in many *M. oryzae* isolates having undergone extensive gene duplication. This may have been facilitated by the presence of *MGR583*, *POT2* and *MAGGY* transposable elements (36, 37) flanking *PWL2* loci, providing the capacity to generate translocations and genomic instability. It is not clear whether the signatures of lineage-specific diversification are due to isolates infecting rice varieties carrying a yet unidentified resistance gene against Pwl2, or resistance genes that have evolved in different host species such as barley cultivars expressing Mla3 or *E. curvula* (14).

We were able to apply CRISPR/Cas9 gene editing in *M. oryzae* to functionally characterise genes occurring in multiple copies through the generation of *Δpwl2* mutants. Our analysis confirmed the previously reported host specificity function of Pwl2, but also revealed it is important for blast disease, with *Δpwl2* mutants showing reduced virulence compared to the isogenic wild type strain. Pwl2 therefore plays an important role during host tissue invasion, consistent with the observation of smaller and fewer disease lesions in susceptible interactions with *Δpwl2* mutants.

Using discovery proteomics, we identified putative Pwl2-interacting proteins, including an isoprenylated small HMA protein, HIPP43, which contains a predicted C-terminal isoprenylation motif. We found that all proteins encoded by the *PWL* gene family can bind HIPP43, including HIPP43 homologs from wheat, rice, weeping lovegrass and foxtail millet. Multiple MAX effectors bind sHMA protein domains, although most previous studies have focused on the incorporation of such domains into paired NLR immune receptors, leading to disease resistance (7, 22, 38, 39). HMA domains are known to be involved in biotic/abiotic stress responses, transport of metals and metal detoxification, and their expression can be organ-specific or tissue-specific within roots, leaves, or stems (40-42). Moreover, sHMAs can localise to the nucleus, plasma membrane, cytoplasm, or plasmodesmata (41, 43, 44), suggesting they might be involved in numerous cellular processes. Consistent with this, sHMAs are expanded in plant genomes with more than 45, and more than 50 sHMA domain-encoding genes occuring in *Arabidopsis* and rice respectively (45). However, little is known about the function of sHMA proteins in plants, especially during plant/microbe interactions, even though they have been reported to act as susceptibility factors (20, 21). For example, deletion mutants of OsHIPP05 (*Pi21*), a proline rich HMA domain protein-encoding gene in rice leads to rice blast resistance (20). Consequently, *pi21* is a recessive resistance gene that

352 has been successfully deployed to control blast disease (20). Similarly, gene silencing or
353 deletion mutants of *TaHIPP1* or *AtHMAD1* in wheat and *Arabidopsis* provide enhanced
354 resistance against *Puccinia striiformis* f. sp. *tritici* and *Pseudomonas syringae* DC3000,
355 respectively (46, 47). In addition, deletion mutants of *AtHIPP27* in *Arabidopsis* lead to
356 increased resistance against cyst nematode (48). However, it is not clear why deletion of sHMA
357 protein-encoding genes impacts immunity. Therefore, the observation that Pwl2 interacts with
358 HIPP43 is revealing, especially as Pwl2 binding appears to enhance its activity, or stability,
359 rather than inhibiting its function. This is consistent with the observation that over-expression
360 of HIPP43 enhances blast susceptibility in rice and barley, respectively.
361 The crystal structure of the Pwl2/HIPP43 complex (presented in the companion paper by
362 Zdrzałek *et al*. (15)) demonstrates that Pwl2 uses an expansive interface to mediate binding to
363 HIPP43, largely using elements of the MAX fold to interact with the β-sheet of the host target.
364 Interestingly, the polymorphic residues found between Pwl2 variants, Pwl2, pwl2-2 and pwl2-
365 3 are not located at the HIPP43 binding interface, but rather located away from the MAX fold
366 on the C-terminal helix of Pwl2. As these polymorphisms are determinants for Pwl2
367 recognition in resistance plants carrying functional cognate resistance gene, it suggests the
368 interface used for immune recognition of Pwl2 in both barley Mla3 lines and resistant weeping
369 love grass are likely spatially distinct from the interface used by Pwl2 to bind to HMA host
370 targets.
371 This observation contrasts with an emerging model where host immune receptors can utilize
372 binding interfaces spatially similar as to those found between effectors and their host targets
373 (38, 39). Indeed, Zdrzałek *et al*. (15) show that if HIPP43 is incorporated into the Pik-1 NLR,
374 in place of its naturally occurring integrated HMA domain, there is potential to gain immune
375 responses to Pwl2. Therefore, we hypothesize Pwl2 may have additional host targets with
376 spatially distinct interfaces from that observed with HIPP43. If true, this may explain
377 differences in Pwl2 HIPP43-binding and immune recognition sites. This suggests immune
378 recognition may have evolved to recognize Pwl2 through interfaces shared with the other
379 undetermined host targets. However, to test this hypothesis, structural information for the
380 natural recognition of Pwl2 by host resistance genes, such as Mla3, or genetic evidence for
381 additional Pwl2 host targets is required.
382 Finally, we show Pwl2 interaction with HIPP43 is important for fungal virulence. A *Δpwl2*
383 null mutant, lacking all three copies of the gene, produced smaller disease lesions that were
384 also fewer in number than caused by the isogenic wild type *M. oryzae* strain Guy11. Moreover,
385 when Pwl2 is over-expressed in transgenic rice or barley, it abolished chitin or flg22-elicited
386 generation of ROS. We also found that over-expression of HIPP43 in rice and barley had a
387 similar effect, suggesting that Pwl2-HIPP43 interaction results in attenuated generation or ROS
388 and reduced immune responses. Consistent with these observations, over-expression of Pwl2
389 or HIPP43 leads to increased susceptibility to *M. oryzae*. How this potential enhancement of
390 HIPP43 activity is stimulated by Pwl2 is not completely clear, but we found that transient co-
391 expression of both Pwl2 and HIPP43 sequestered HIPP43 away from plasmodesmata, with the
392 two proteins co-localizing in the cytoplasm and in large mobile vesicular bodies. The sub-
393 cellular localization of Pwl2 and HIPP43 was distinct when separately expressed, with Pwl2
394 accumulating in the cytoplasm and mobile bodies while HIPP43 localized to the membrane,
395 and particularly to plasmodesmata. Deletion of the isoprenylation motif abolishes PD
396 localization showing the C-terminal isoprenylation motif is important for plasmodesmatal (PD)
397 localization. This suggests that disrupting PD localization may lead to HIPP43 translocation to
398 other organelles, which may in-turn influence immune signaling.
399 Localization of HIPPs at PD has been previously reported. HIPP7 and HIPP26 localise at PD,
400 and this localisation can be altered by mutations in the isoprenylation motif (44, 49). Although
401 characterised HIPPs through their HMA domains are thought to be metallochaperones, there

402 are no studies that link metal detoxification and immunity. Some studies suggest that there may
403 be a connection between concentration of metal ions, such as iron, copper, cadmium and zinc
404 and plasmodesmatal permeability (50). This might explain why a plant pathogen effector
405 targets a plasmodesmatal localized HIPP. Both the HMA domain and the isoprenylation
406 regions of HIPPs have been shown to be important in plant immunity. For example, a mutation
407 targeting the proline-rich region of *pi21* is sufficient to lead to gain of resistance against *M.*
408 *oryzae (20)*, while interfering with the isoprenylation of HIPP1-V from wild wheat (*H. villosa*)
409 leads to loss of resistance against *Blumeria graminis* f. sp. *tritici* accompanied by reduced
410 localization to PD. Interestingly, HIPP1-V interacts with the E3-ligase CMPG1 at the plasma
411 membrane leading to resistance against powdery mildew in an isoprenylation-dependent
412 manner (51). This interaction has been reported to activate expression of genes involved in
413 ROS generation and salicylic acid biosynthesis, suggesting that HIPP1-V is required for PTI
414 regulation (51) An *A. thaliana* HIPP3 has also been proposed to be involved in regulation of
415 the pathway involved in salicylic-dependent plant immunity via LSD1, PAD4 and SAG101
416 (40).
417 The change in cellular localization of HIPP43 induced by Pwl2 may therefore inhibit its
418 function in immunity or lead to a new role that enhances disease susceptibility. Future work
419 will be necessary to see if HIPP43 directly regulates ROS generation or acts in a more indirect
420 manner through binding other signaling components involved in PTI. By dislocating HIPP43
421 from the PD, Pwl2 may attenuate a role for HIPP43 in PD immunity. Pwl2 is a highly mobile
422 effector and has been shown to move into neighbouring rice cells ahead of *M. oryzae* hyphal
423 growth (23). This has been suggested to be a step to prepare un-invaded cells for fungal
424 colonisation. Its role may therefore be to alter the sub-cellular localisation, concentration and
425 stability of HIPP43, enabling more rapid tissue colonisation by the blast fungus.
426

Acknowledgements

We thank current and past members of the "BLASTOFF" team from the Banfield, Kamoun, Terauchi, Talbot, and Moscou Laboratories. For funding, we thank Gatsby Charitable Foundation and Biotechnology and Biological Sciences 462 Research Council (BBSRC) BBS/E/J/000PR9797 and a BBSRC grant to NJT and FLHM 463 (BB/V016342/1 and 101077853 "PANDEMIC"). United States Department of Agriculture-Agricultural Research Service CRIS #5062-21220-025-000D (MJM. We acknowledge Y.K Gupta, J.C De la Concepcion, J. Rhodes and J. Win for constructive discussions.

Author Contributions

Conceptualization: NJT and VW
Formal analysis: VW, XY, AF, JK, JS, DG, TL, YPH, ABE, MS, MJB, WM and RZ
Funding acquisition: NJT
Investigation VW, XY, AF, JS, DG, AG, DK, YPH, ABE, MJB, WM and RZ
Writing – original draft: VW and NJT
Writing – review & editing: VW, NJT, LR, AB, TL, MB, SK, MM, FM

445 **Materials and methods**

446 **Fungal strains, growth conditions and infection assays**

447 Fungal isolates were routinely grown on complete medium (CM) at 24°C with a controlled 12
448 h light and dark cycle for up to 12 days (52). *H. vulgare*, *E. curvula* and *O. sativa* plants were
449 grown for 7, 14 and 21 days respectively in 9 cm diameter plastic plant pots or seed trays.
450 Conidia were recovered from 10-day old cultures using a sterile disposable plastic spreader in
451 3 mL sterile distilled water. The conidial suspension was filtered through sterile Miracloth and
452 centrifuged at 5000 x g for 5 min at room temperature and adjusted to a final of concentration
453 of 1 x10^5 conidia mL^{-1} in 0.2 % gelatin. The spore suspension was used for spray or leaf drop
454 infections assays. After spray inoculation, the plants were covered in polythene bags and
455 incubated in a controlled plant growth chamber at 24°C for 48 h with a 12 h light and dark
456 cycle, and 85% relative humidity, before removing the polythene bags. The inoculated plants
457 were incubated for 3 more days before scoring the lesions. For each treatment 10 leaves were
458 collected before counting typical disease lesions that are characterised by ellipsoid necrotic
459 lesions with a grey centre, on the leaf surface (53). Each experiment was repeated minimum of
460 three times, yielding consistent outcomes.

461 **Leaf infection assay and live-cell imaging**

462 Rice leaf sheaths from 4 weeks old susceptible cultivars Moukoto or CO39 were inoculated
463 with 4 mL of a suspension at 5 x 10^4 of conidia mL^{-1} in distilled water using a micropipette as
464 described in Kankanala et al 2007 (25). The inoculated leaf sheaths were incubated at 24°C for
465 at least 24 h before a thin layer of the inner leaf sheath was dissected using a blade and mounted
466 on a glass slide. Live cell imaging was carried out on an IX81 motorized inverted microscope
467 (Olympus, Hamburg, Germany) for conventional and differential interference contrast (DIC)
468 microscopy using the Photometrics CoolSNAP HQ2 camera (Roper Scientific, Germany).
469 Images were analyzed using ImageJ. For Leica SP8 laser confocal microscopy, settings were
470 as follows; GFP, YFP and RFP/mCherry tagged proteins were excited using 488, 514 and 561
471 nm laser diodes and the emitted fluorescence detected using 495-550, 525-565 and 570-620
472 nm respectively. The auto-fluorescence from chlorophyll was detected at 650-740 nm.

473 **Generation of fungal transformation plasmids**

474 Single or multiple DNA fragments were cloned into fungal transformation vector using In-
475 Fusion HD Cloning Kit (Clontech, USA). Briefly, fragments from cDNA, genomic DNA or
476 synthesized DNA were amplified using primers that introduce a 15bp overhang complementary
477 to sequences at the restriction sites of the destination vector or adjacent insert fragments. This
478 allows the ends to fuse by homologous recombination during cloning. Positive transformation
479 was accessed using colony PCR and constructs sequenced then analysed on SnapGene. A list
480 of primers is provided in Table S3.

481 **RNA isolation, RNA sequencing and analysis**

482 To study *in-planta* gene expression profile of *PWL2* and other effectors, leaf drop infection
483 assays were carried out on a susceptible rice line Moukoto and samples collected at 24 and 72
484 hpi. Infected plant material was ground into fine powder using a sterile nuclease-free mortar &
485 pestle containing liquid nitrogen. RNA was isolated from *M. oryzae* mycelia inoculated or rice
486 leaves using QIAGEN RNeasy Plant Mini Kit according to manufacturer's instructions. The
487 RNA quality was determined on a NanoDrop spectrophotometer (Thermo Scientific, UK) and
488 Agilent 2100 Bioanalyser using an RNA nano-chip kit (Agilent Technologies, UK). Library
489 preparation was carried out using Illumina® sequencing TruSeq Stranded Total RNA Library

490 Prep Kit before sequencing of 100 bp paired ends reads using Illumina Genome Analyser GXII
491 platform by the Exeter Sequencing Service (University of Exeter). *M. oryzae* specific reads
492 were recovered as unmapped reads after mapping to the *O. sativa* L. ssp. japonica genome
493 (IRGSP-1.0) (54). To determine differentially genes expression, reads were then mapped to
494 transcripts from the M. oryzae 70-15 reference genome (55) or a laboratory strain KE002 using
495 TopHat2 splice site-aware aligner (56). Differential expression analysis was carried out using
496 DESeq2 packages (57). .

497 **Generation of Cas9-sgRNA targeted gene deletion**

498 A sgRNA was designed for CRISPR-Cas9 genome editing using an online tool E-CRISP
499 http://www.e-crisp.org/E-CRISP/. A 20-nucleotide sequence was selected at the *PWL2* locus
500 (not including the PAM NGG-sequence). The sgRNA was first synthesised using the EnGen
501 sgRNA synthesis kit New England Biolabs (NEB #E3322) before mixing with the Cas9-NLS
502 to form the RNP complex. The mixture was incubated at room temperature for 10 min before
503 fungal transformation. *M. oryzae* protoplast were generated as described by Talbot *et al* (52).
504 The RNP complex together with the donor template was mixed with Guy11 protoplasts re-
505 suspended in 150 µL of STC to a concentration of 1 X 10^8 and incubated at room temperature
506 for 25 min before adding 60% PEG. Successful transformants were selected on complete media
507 (CM) agar containing Hygromycin B to a final concentration of 200 µg mL^{-1}.

508 **Southern blot blotting**

509 This procedure was adapted from the protocol of Southern (58) with adjustments as described
510 by Sambrook *et al* (59). Fungal genomic DNA (15 µg) was digested with the appropriate
511 restriction enzyme overnight at 37°C. The digested genomic DNA was then separated by gel
512 electrophoresis. The DNA embedded in the agarose gel was de-purinated by immersion in 0.25
513 M HCl before transferring the DNA onto Hybond-NX membrane (Amersham Biosciences).
514 The membrane was exposed to UV light in a BLX-254 cross linker (Bio-Link®) to fix and
515 immobilise the DNA. The membrane was then probed overnight using a DIG-labelled PCR
516 product in freshly prepared hybridization buffer (25-50ng mL) in a 50 mL falcon tube.
517 Chemiluminescent detection of DIG-labelled DNA was carried using CDP-Star solution
518 (Roche) before detection.

519 **Whole genome sequencing**

520 Purified RNA-free DNA was obtained using Hexadecyltrimethylammonium Bromide
521 (CTAB). Template quality was assessed using a NanoDrop spectrophotometer and Qubit.
522 Sequencing was carried out at Exeter Sequencing services (University of Exeter, UK) and
523 Novogene (Cambridge, UK). NEXTflex™ Rapid DNA-seq Library Prep Kit was used to
524 prepare and index libraries before sequencing on HiSeq 2500 (Illumina) with two lanes per
525 sample. The quality of sequencing reads was first checked using the FastQC toolkit
526 (http://www.bioinformatics.bbsrc.ac.uk/projects/fastqc/). From the raw data (fastq files),
527 adaptor sequences were trimmed from sequences containing adaptors and low-quality reads
528 removed using the fastq-mcf program. The trimmed sequences were aligned to the reference
529 genome (70-15) (55) using BWA (Burrow Wheeler Aligner) https://github.com/lh3/bwa (60).
530 Bam files were visualized on IGV genome viewer to determine CRISPR gene deletion.

531 **Copy number variation of *PWL2***

532 A total of 286 *M. oryzae* isolates with raw Illumina-based sequencing information were
533 downloaded from NCBI (performed on October 16th, 2019). Copy number variation was
534 assessed using a k-mer analysis approach using the k-mer analysis toolkit (KAT; v2.4.1).
535 Coding sequence information for *M. oryzae* isolate 70-15 were used as template for k-mer
536 analysis and raw Illumina reads were input. Default parameters were used including k-mer of
537 length 27 nt. Copy number variation of individual effectors is based on average k-mer coverage
538 as compared with the median coverage for all genes.

539 **Phylogenetic analysis of *Magnaporthe***

540 Genome sequences of diverse *M. oryzae* isolates were identified based on literature review and
541 search on NCBI (performed on August 9th, 2019). For isolates having only Illumina sequencing
542 data, raw paired reads were downloaded from NCBI, trimmed using Trimmomatic (v0.36)
543 using the parameters: removing of adapters with ILLUMINACLIP:TruSeq2-PE.fa:2:30:10,
544 remove leading low quality or N based with quality below 5 for leading (LEADING:5) and
545 trailing sequence (TRAILING:5), scan and cut reads with 4 bp sliding window below 10
546 (SLIDINGWINDOW:4:10), and minimum length of 36 bp (MINLEN:36). KmerGenie
547 (v1.7048) was used to identify an optimal k-mer for genome assembly using default
548 parameters. Genome assembly was performed using minia (v0.0.102) with default parameters.
549 kSNP3 (v.3.021) was used to develop a phylogenetic tree of *M. oryzae* using assembled
550 genomes as input with parameters of k-mer of 29 bp and minimum fraction of 0.4. The
551 phylogenetic tree was generated using RAxML (v) using the General Time Reversible model
552 of nucleotide substitution under the Gamma model of rate heterogeneity.

553 **Generation of *Agrobacterium* transformation plasmids**

554 Single or multiple DNA fragments were cloned into binary vector using In-Fusion HD Cloning
555 Kit (Clontech, USA). Briefly, fragments from cDNA were amplified using primers that
556 introduce a 15bp overhang complementary to sequences at the restriction sites of the
557 destination vector or adjacent insert fragments. Alternatively synthesized DNA fragments were
558 designed to have 15bp overhang complementary to sequences at the restriction sites of a binary
559 vector pG514 customized for infusion cloning by digesting with either *Xba*1 and *Pca*1 or *Sac*1
560 (New England Biolabs) to remove the *ccDB* toxin encoding gene. Positive transformation was
561 accessed using colony PCR and constructs sequenced and analyzed on SNAP gene.

562 **Transient expression in *Nicotiana benthamiana***

563 *Agrobacterium tumefaciens* strain *GV3101* (61) was used for transient expression. Three-week-
564 old *N. benthamiana* leaves were infiltrated with transformed *Agrobacterium* carrying T-DNA
565 constructs, expressing the gene of interest. Bacterial cultures were diluted to obtain a final OD
566 600nm of 0.4 in agroinfilitration buffer (10mM MES, 10 mM $MgCl_2$, 150 µM acetosyringone,
567 pH 5.6). Leaf discs were cut from agroinfiltrated tissue 48 hpi and subjected for microscopy or
568 used co-IP.

569 **Plant transformation and ROS measurement**

570 *Agrobacaterium tumefaciens* strain *AGL1* (61) was used for plant transformation as described
571 in (62). Positive transgenics plants were first selected on hygromycin followed by confirmation
572 using PCR. Alternatively, leaf discs were collected from transgenic plants and analysed for
573 copy number at iDNA Genetics Ltd (Norwich, UK) to detect hygromycin insertion events. In
574 addition, expression of the protein was evaluated using SDS-PAGE. To measure response to

575 PTI elicitors, a 4-mm diameter biopsy punch (Integra™ Miltex ™) was used to cut leaf discs
576 from 5 weeks old *H. vulgare* and *O. sativa* transgenic plants. The leaf discs were transferred
577 into 96-well-plates (Greiner Bio-One) containing 100 µL of distilled H_2O in each well and
578 incubated overnight at room temperature. The assay was carried out by replacing the distilled
579 H_2O in the wells by a 100 µL reaction solution of 100 µM Luminol or L-012 (Merck), 20 µg
580 mL^{-1} horseradish peroxidase (Merck) together with elicitors, flg22 (1 µM final concentration),
581 chitin (1mg/mL final concentration) or without (mock). The photon count was carried out using
582 the (HRPCS218, Photek) equipped with a 20 mm F1.8 EX DG ASPHERICAL RF WIDE
583 LENS (Sigma Corp). Each experiment was repeated three times conducted a minimum of three
584 times, yielding consistent outcomes.

585 **Co-immunoprecipitation and sample preparation for mass spectrometry**

586 Leaves were harvested from two-three weeks old barley transgenic plants and rapidly frozen
587 in liquid nitrogen before storage or immediately ground into fine powder using a
588 GenoGrinder® tissue homogenizer. Ground powder was quickly transferred into ice-cold 1.5
589 mL Eppendorf tube and 2 mL of ice-cold extraction buffer (GTEN [10% (v/v) glycerol, 25 Mm
590 Tris pH 7.5, 1 mM EDTA 150 mM NaCl, 2% (w/v) PVPP, 10 Mm DTT, 1 X protease inhibitor
591 cocktail (Sigma), 0.5% (v/v) IGEPAL added and mixed thoroughly. This was centrifuged at
592 3000 x g for 10 min at 4°C to recover total proteins in the supernatant and repeated twice. A
593 volume of 2 mL of total protein was mixed with 25 µL of GFP-TRAP agarose beads (50%
594 slurry, ChromoTek) and incubated shaking overnight at 4°C. The GFP-TRAP agarose beads
595 were centrifuged for 2 min at 3000 x g before washing three times with wash buffer
596 (ChromoTek). Bound proteins were recovered by resuspending the beads in loading buffer
597 (loading dye, 10 mM DTT, H2O) and incubated at 70°C for 10 minutes. An aliquot of the
598 sample was run on SDS-PAGE gel and used for Western blotting (63). Recovered proteins
599 from co-immunoprecipitation were run on an SDS-PAGE gel for approximately 1 cm. The gel
600 was washed for 1 h in distilled water followed by 1 incubation SimplyBlue™ Safe stain. The
601 gel was then washed three times in distilled water the region containing proteins excised using
602 a scalpel.

603 **Mass spectrometry and data processing**

604 Protein purification, immunoprecipitation, sample preparation, liquid chromatography
605 followed by tandem mass spectrometry (LC-MS/MS), and data analysis were previously
606 described in full detail (64). Briefly proteins identified in immunoaffinity-enriched samples
607 were measured with data dependent method on high resolution LC-MS systems, Orbitrap
608 Fusion (Thermo Ltd). The acquired spectra were peak-picked and searched by Mascot search
609 engine (Matrix Science Ltd) to identify the peptide sequences from the search space defined
610 by the background proteome. The peptides were combined into proteins based on the principle
611 of parsimony by the search engine. Resulting proteins were further described by quantitative
612 values based on the number of spectra that identify them. The individual runs were combined
613 in the Scaffold program (Proteome Software Inc.), where the data were evaluated and filtered
614 to contain less than 1% false positives (FDR) and resulted matrix exported as a spreadsheet.
615 The matrix of proteins detected in different samples serves as the input for an R script for
616 further processing and visualization.

617 **Yeast two-hybrid analysis**

618 To clone genes of interest into bait (pGBKT7 DNA-BD cloning) vector or prey (pGADT7
619 activating domain) vector, using the In-Fusion HD Cloning Kit (Clontech) kit. The bait and
620 prey vectors were digested using vector was digested using *Bam*H1 and *Eco*R1 while the gene

621 to be inserted was PCR-amplified using primers containing 15 bp overhangs with homology to
622 the two ends of the digested bait vector. For transformation, a single colony Y2H gold yeast
623 strain was mixed in 1 mL of liquid yeast extract peptone dextrose (YPD). Competent cells were
624 prepared as described in manufactures transformation protocol (Zymo Research). Briefly, for
625 transformation 700 ng – 1 µg of plasmids expressing Pwl2 or other effectors in pGADT7 and
626 *Hv*HIPP43 or plant proteins in pGBKT7 were co-transformed in competent cells and Frozen-
627 EZ Yeast Solution 3 added before incubation at 28ºC for 1 h and transformed cells plated on
628 selection media lacking Leucine (L) and Tryptophan (W) and incubated at 28º C for 3-5 days.
629 To detect interactions the colonies were transferred to media lacking Leucine (L), Tryptophan
630 (W), Adenine (A) Histidine (H), Bromo-4-Chloro-3-Indolyl a-D-galactopyranoside (X-a-gal)
631 and 10 mM 3-amino-1,2,4-triazole (3AT) (Sigma). The plates were imaged after 60-72
632 incubation at 28ºC. Each experiment was conducted a minimum of three times, yielding
633 consistent outcomes.

634 ***In-planta* co-immunoprecipitation (co-IP)**

635 To test interaction of protein *in planta*, genes of interest tagged with either GFP or Myc were
636 cloned into the vector pGW514 and transformed into *Agrobacterium* strain *GV301* and co-
637 infiltrated (OD_{600} = 0.4 for effectors and OD_{600} = 0.6 for HIPP43) into 3 to 4-week-old *N.*
638 *benthamiana* leaves and incubated for 48 h to allow protein expression. Total protein was
639 isolated in ice-cold extraction buffer (GTEN [10% (v/v) glycerol, 25 Mm Tris pH 7.5, 1 mM
640 EDTA 150 mM NaCl], 2% (w/v) PVPP, 10 Mm DTT, 1 X protease inhibitor cocktail (Sigma),
641 0.5% (v/v) IGEPAL). Total protein was co-immunoprecipitated using the anti-GFP M2 resin
642 (Sigma-Aldrich, St. Louis, MO) and washed 3 times using immunoprecipitation buffer before
643 analyzing on an SDS-PAGE gel. Recovered proteins from co-immunoprecipitation were
644 separated on an SDS-PAGE gel and transferred onto a polyvinylidene diflouride (PVDF)
645 membrane using a Trans-Blot turbo transfer system (Bio841 Rad, Germany). Detection was
646 performed using the appropriate antibody either anti-GFP-HRP or anti-Myc-HRP. Imaging
647 was carried out using an ImageQuant LAS 4000 luminescent imager (GE Healthcare 844 Life
648 Sciences, Piscataway, NJ, U.S.A.) according to manufacturer's instructions.

649 **Sub-cellular localization and plasmodesmata quantification**

650 Leaf discs were obtained from *N. benthamiana* plants agroinfiltrated with different construct
651 combinations at 24 and 48 hpi and mounted on a slide immersed in perfluorodecalin and
652 observed using X63 oil immersion lens. For Leica SP8 laser confocal microscopy, settings
653 were as follows; GFP, YFP and RFP/mCherry tagged proteins were excited using 488, 514,
654 and 561 nm laser diodes and the emitted fluorescence detected using 495-550, 525-565, and
655 570-620 nm respectively. The auto-fluorescence from chlorophyll was detected at 650-740 nm.
656 To stain and quantify plasmodesmata, agroinfiltrated leaves were further infiltrated with 0.1%
657 aniline (Sigma-Aldrich #415049, in PBS buffer, pH 7). Images were analyzed using ImageJ to
658 determine the number of plasmodesmata. First, cell peripheries were divided into 20 µm
659 sections and the number of plasmodesmata determined per 20 µm.

660 **Phylogenetic analysis of grass HMA proteins**

661 Proteins from *B. distachyon* (314; v3.1), *H. vulgare* (Jul2020), *T. aestivum* (RefSeqv2.1; 09-
662 16-2020), *O. sativa* (323; v7.0), *Oropetium thomaeum* (386; v1.0), *Sorghum bicolor* (454;
663 v3.1.1), *Setaria italica* (312; v2.2), and *Zea mays* (RefGen_V4) containing an HMA domain
664 were identified using InterProScan (v5.59-91.0; Pfam PF00403). The HMA domain was
665 extracted using the script QKdomain_process.py including an additional 10 amino acid
666 sequences N and C-terminal of the Pfam boundaries (-n 10 -c 10). The non-redundant set of

667 HMA domains were identified using CD-HIT (v.4.8.1) with parameter -c 1.0. Structure guided
668 multiple sequence alignment was performed using MAFFT with parameters dash, max iteration
669 of 1000, and globalpair. Maximum likelihood phylogenetic analysis was performed using
670 RAxML (v8.2.12) using the Gamma model of rate heterogeneity, JTT amino acid substitution
671 model, and 1,000 bootstraps. Coding sequence was identified for the HIPP43 gene family and
672 aligned using MUSCLE (v5) translation alignment using default parameters. Maximum
673 likelihood phylogenetic analysis was performed using RAxML (v8.2.12) using the General
674 Time Reversible model of nucleotide substitution under the Gamma model of rate
675 heterogeneity and 1,000 bootstraps.

676 **Statistical analysis and Protein structure prediction using AlphaFold2**

677 Significance difference between groups of samples was performed using GraphPad Prism 10.
678 P values < 0.05 were considered significant, ****P<0.0001, ***P<0.001, **P<0.01 while
679 values P values > 0.05 were considered as non-significant in an unpaired Student's t-test.
680 Structure prediction was carried out using AlphaFold2 and the structure analyzed, and figures
681 made using ChimeraX

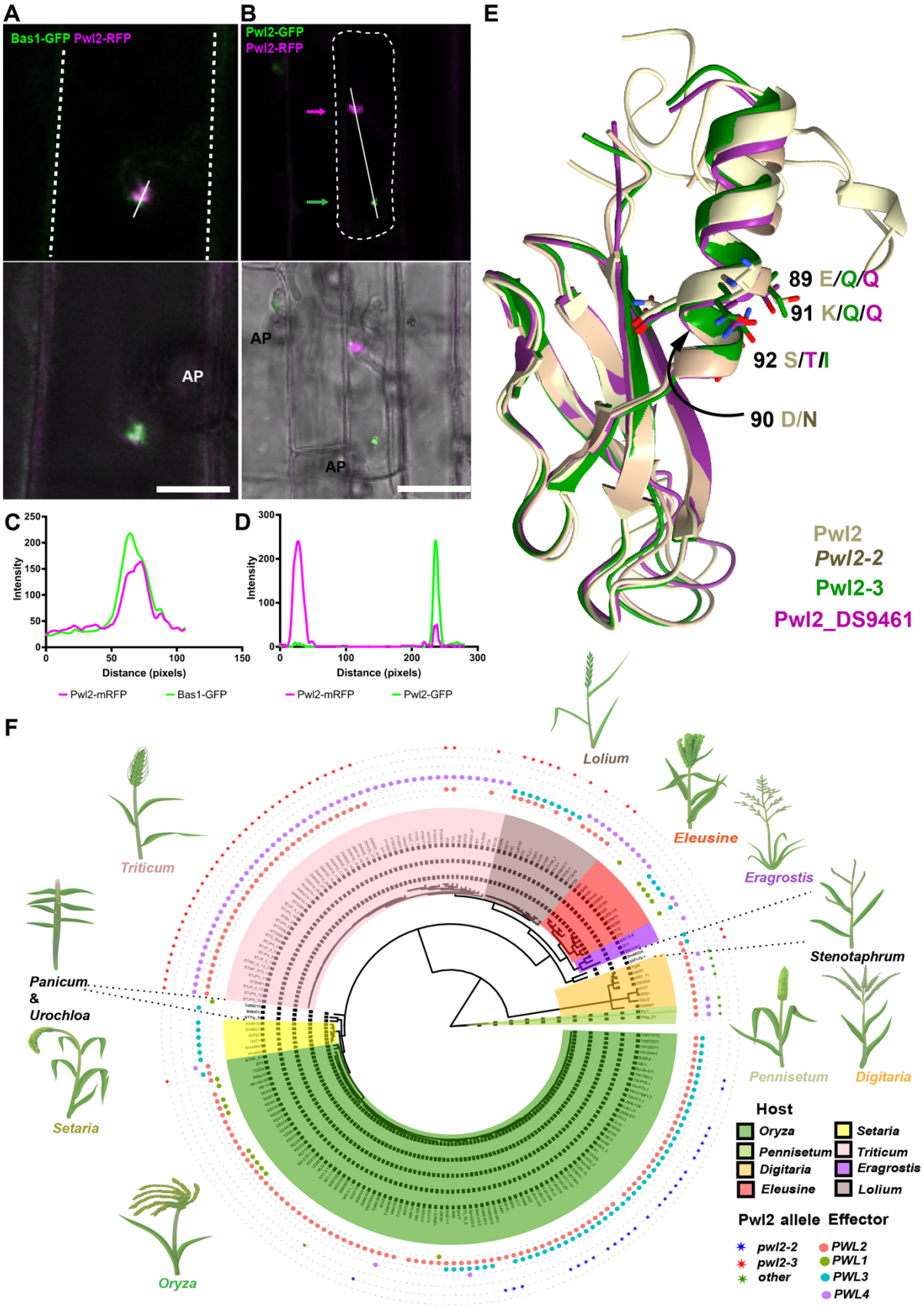

682
683
684
685

686 **Fig. 1**. **Pwl2 is a BIC localized effector that is ubiquitous in isolates of *M. oryzae* and**
687 **displays conserved structural features.**
688 (*A+C*) Micrographs showing Pwl2 secreted through the Biotrophic Interfacial Complex (BIC)
689 in rice cells during early infection. Conidial suspension at 1X 10^5 mL^{-1} of *M. oryzae* strain co-
690 expressing Bas1-GFP and Pwl2-mRFP were inoculated onto a susceptible cultivar Moukoto
691 rice leaf sheath and images captured at 26 hpi. Fluorescence of the two effectors was observed
692 as small punctate signals in the same BIC. (*C+D*) Co-infection assay of rice leaf sheath with
693 *M. oryzae* strains expressing Pwl2-mRFP and Pwl2-GFP at 30 hours post-infection (hpi).
694 Micrographs and line scan graph shows there is an absence of mixed fluorescence confirming
695 the BIC does not contain Pwl2 transferred from rice cells. BICs indicated by magenta arrows
696 for mRFP and green arrows for GFP. (*E***)** Superimposition of different Pwl2 variants predicted
697 using AlphaFold2 onto the resolved Pwl2 structure (companion paper to this study by Zdrzalek
698 *et al* (15)) indicating region of polymorphism. (*F***)** Phylogenetic analysis and *PWL* gene family
699 distribution in *M. oryzae*. A maximum parsimony tree including *M. oryzae* strains and isolates
700 from related species *Magnaporthe grisea* and *Pyricularia pennisetigena*. The heatmap
701 indicates the presence/absence of genes in the *PWL* family. *PWL1* is found in *Eleusine* and
702 *Oryza* lineages. *PWL2* is conserved across various *M. oryzae* lineages and isolates infecting
703 crabgrass and pearl millet. *PWL3* is specific to *Oryza*, *Lolium*, *Setaria*, and *Eleusine* lineages.
704 *PWL4* is predominantly found in *Eleusine*, *Eragrostis*, *Lolium*, and *Triticum* lineages.
705 Maximum parsimony tree of *M. oryzae* isolates was generated using a standalone, whole
706 genome multiple alignment/SNP calling program, kSNP3. We used *Pwl1, Pwl2, Pwl3* and
707 *Pwl4* protein sequence to query for presence/absence polymorphism of the gene families using
708 tblastn.
709

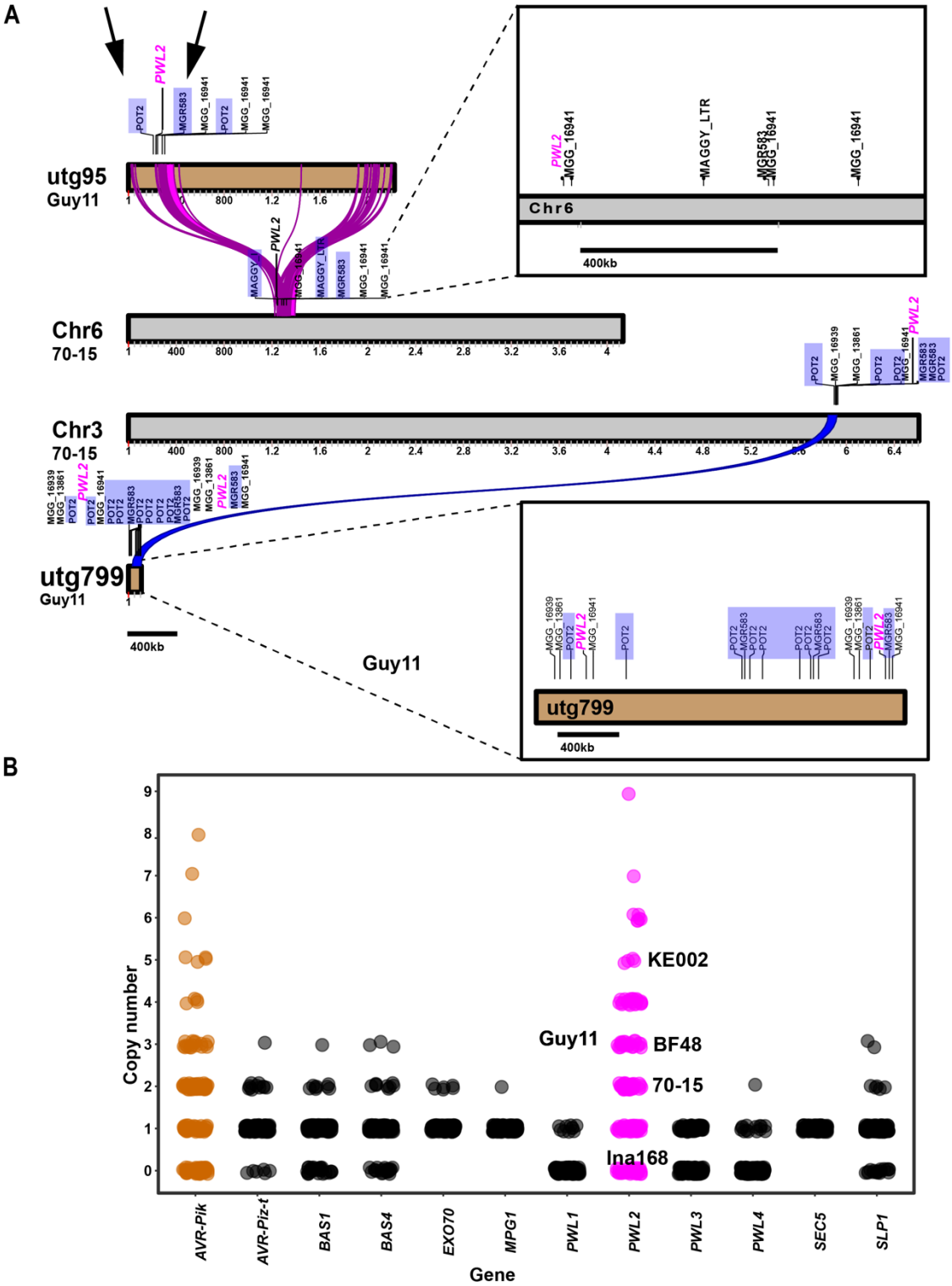

Fig. 2. *PWL2* occurs in multiple loci and shows high copy number variations in field isolates.

(*A*) Schematic showing the estimated chromosomal location of *PWL2* on multiple loci (Chr3 and 6) of the reference genome 70-15 and on equivalent region of assembled contigs of laboratory strain Guy11 genome. *PWL2* is flanked by *POT2* and *MGR583* repeated sequences suggesting a possible involvement in translocation of events into different loci in the genome. Arrows indicate location of *PWL2*. (*B*) A k-mer analysis on sequenced raw reads was used to

719 determine copy number variation of *PWL* family genes in different *M. oryzae* isolates. Plot
720 shows high copy number of *PWL2* in analyzed genomes (n = 286) compared to the other *PWL*
721 gene family members, another effector *SLP1,* and selected control genes *MPG1* and *SEC5*.
722 Similarly, *AVR-Pik* shows multiple copies in different isolates. Copy number of *PWL2* in
723 selected isolates Guy11, KE002, BF48, 70-15 is indicated with Ina168 that lack *PWL2* used as
724 a negative control.
725
726

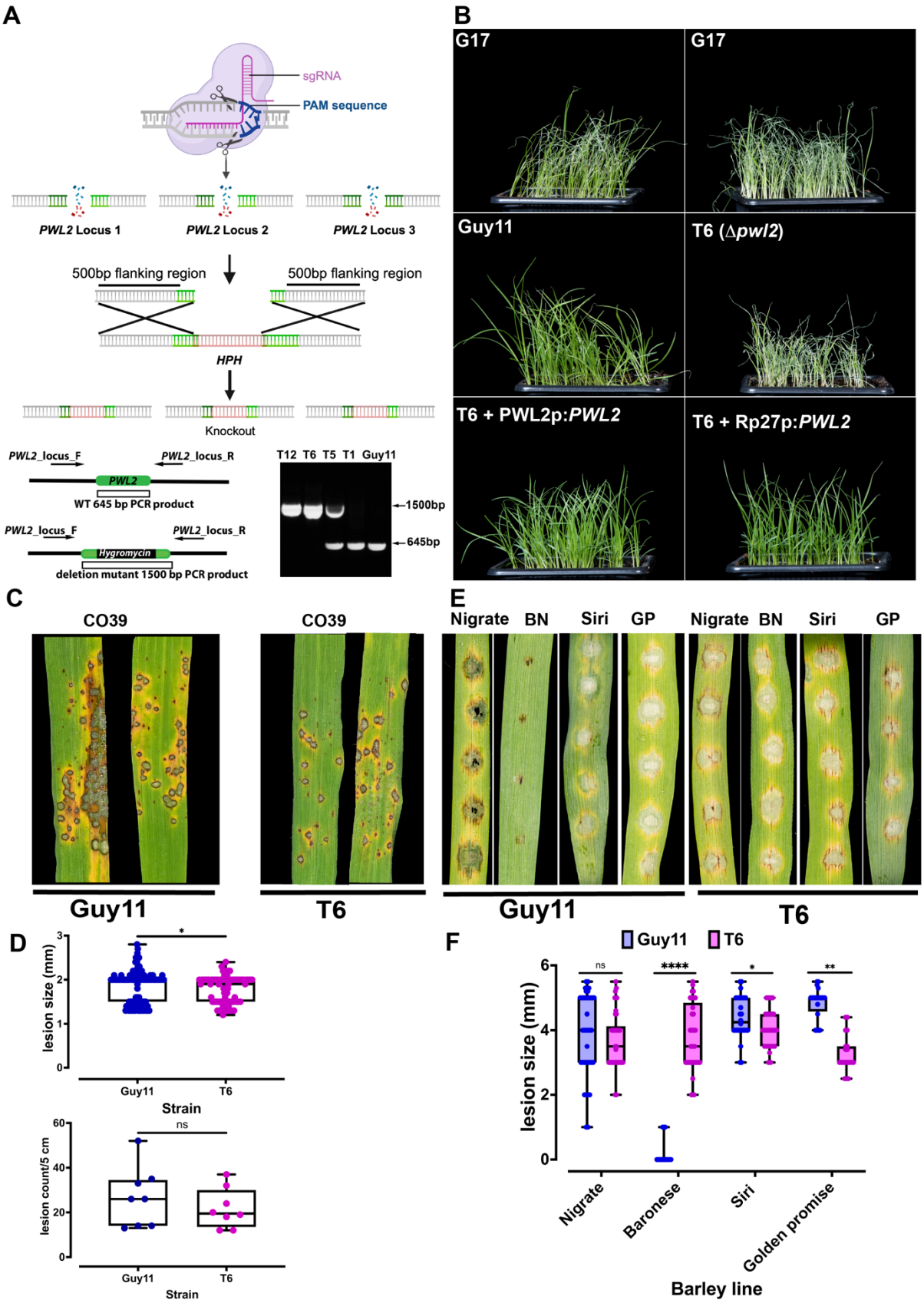
A
sgRNA
PAM sequence
PWL2 Locus 1
PWL2 Locus 2
PWL2 Locus 3
500bp flanking region
500bp flanking region
HPH
Knockout
PWL2_locus_F
PWL2_locus_R
PWL2
WT 645 bp PCR product
PWL2_locus_F
PWL2_locus_R
Hygromycin
deletion mutant 1500 bp PCR product
T12 T6 T5 T1 Guy11
1500bp
645bp
B
G17
G17
Guy11
T6 (Δpwl2)
T6 + PWL2p:PWL2
T6 + Rp27p:PWL2
C
CO39
CO39
Guy11
T6
E
Nigrate BN Siri GP
Nigrate BN Siri GP
Guy11
T6
D
lesion size (mm)
Guy11
T6
Strain
lesion count/5 cm
ns
Guy11
T6
Strain
F
Guy11 T6
lesion size (mm)
ns
****
*
**
Nigrate
Baronese
Siri
Golden promise
Barley line

Fig. 3. CRISPR-Cas9 *Δpwl2* mutants demonstrate gain of virulence on weeping lovegrass and barley carrying *Mla3*.

(*A*) Schematic illustration of the CRISPR-Cas9 mediated gene editing process for inserting the Hygromycin Phosphotransferase (*HPH*) gene cassette at the *PWL2* locus. The guided sequence (sgPWL2) directs Cas9 to introduce a double stranded break at the *PWL2* locus, with the DNA repair template containing the Hygromycin resistance gene cassette and flanking regions of the *PWL2* gene. This leads to mutations in the form of indels or gene replacements. Figure created with BioRender https://biorender.com/. Positive transformants were identified by amplifying the *PWL2* coding sequence from the wild type Guy11 and the hygromycin cassette from transformants with the three copies deleted. (*B*) Comparison of disease symptoms in weeping lovegrass (*Eragrostis curvula*) infected with different *M. oryzae* isolates. In the top panel, typical disease lesions produced by *E. curvula*-infecting isolate G17 are shown. In the middle panel, CRISPR-Cas9 deletion mutants exhibit gain of virulence on weeping lovegrass compared to Guy11. In the bottom panel, complemented strains with both native and constitutive RP27 promotors showed a loss of virulence on weeping lovegrass. (*C*) *Δpwl2* mutants display reduced pathogenicity on rice cultivar CO39. Conidial suspensions at 1×10^5 mL^{-1} spores/mL from Guy11 and *Δpwl2* T6 were used to inoculate 21-d-old seedlings of the blast-susceptible cultivar CO39, and disease symptoms recorded after 5 dpi. (*D*) The box plots show the lesion size (top) and lesion density (bottom) of seedlings infected with Guy11 and *Δpwl2* T6. The lower horizontal line shows the minimum value, and the upper horizontal line shows the maximum value. The lower border and upper border of the box show the lower quartile and upper quartile, respectively. The line in the box shows the median. (*E*) The *Δpwl2* mutant exhibits enhanced pathogenicity on barley cultivar Baronesse (*Mla3*). Conidial suspensions at 1×10^5 mL^{-1} spores/mL from Guy11 and *Δpwl2* T6 were used to inoculate 10-day old seedlings of barley lines Golden Promise, Siri, Nigrate and Baronesse, and disease symptoms recorded after 5 dpi. (*F*) The box plot shows lesion size of barley seedlings infected with Guy11 and *Δpwl2* T6. The lower horizontal line shows the minimum value, and the upper horizontal line shows the maximum value. The lower border and upper border of the box shows the lower quartile and upper quartile, respectively. The line in the box shows the median. Significance between groups of samples was performed using Unpaired Student's t-test. ****$P<0.0001$, **$P<0.01$, $P<0.05$, NS indicates no significant difference.

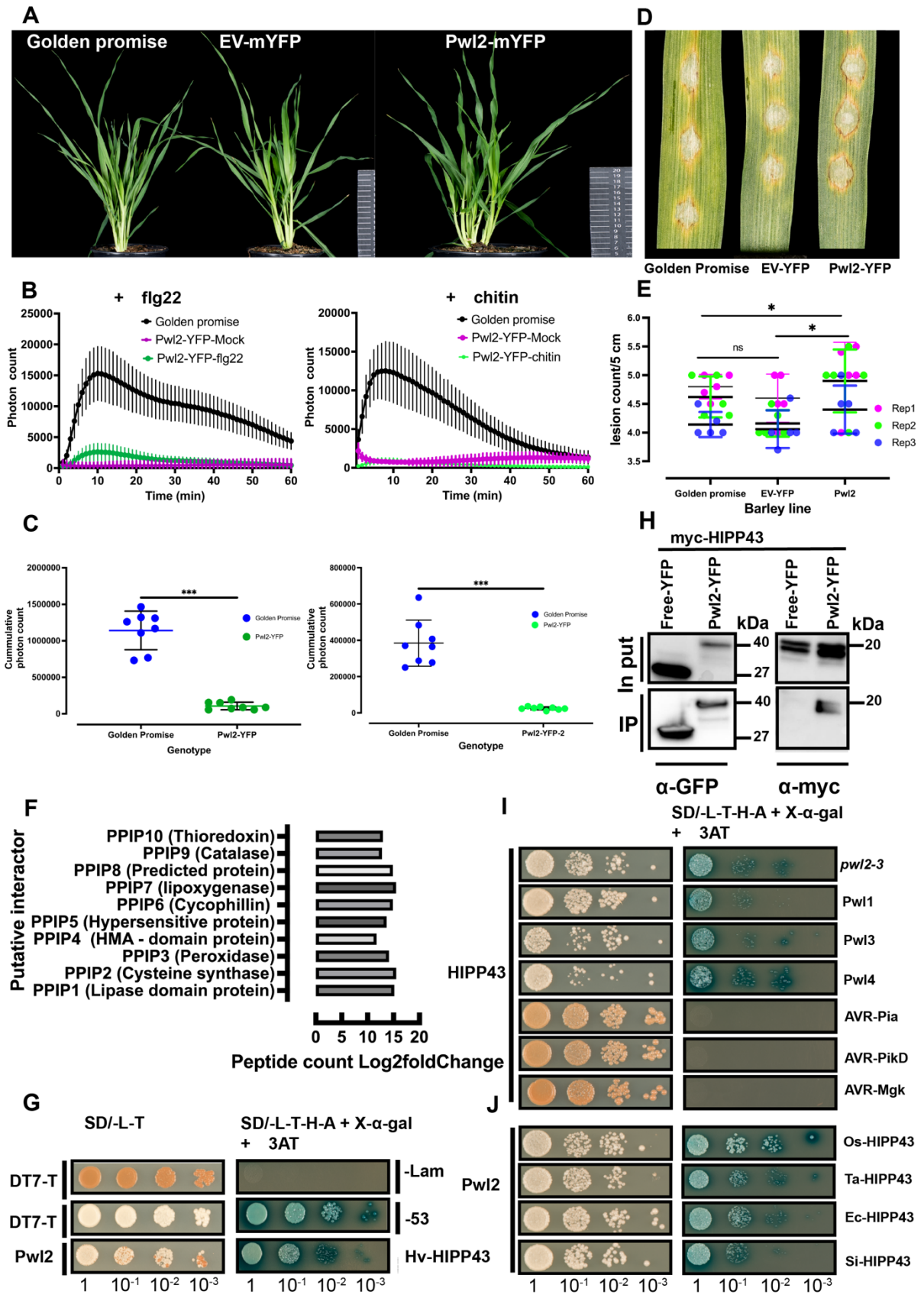
A
Golden promise
EV-mYFP
Pwl2-mYFP
D
Golden Promise
EV-YFP
Pwl2-YFP
B
+ flg22
Golden promise
Pwl2-YFP-Mock
Pwl2-YFP-flg22
Photon count
Time (min)
+ chitin
Golden promise
Pwl2-YFP-Mock
Pwl2-YFP-chitin
Photon count
Time (min)
E
lesion count/5 cm
ns
*
*
Rep1
Rep2
Rep3
Golden promise
EV-YFP
Pwl2
Barley line
C
Cummulative photon count
***
Golden Promise
Pwl2-YFP
Genotype
Cummulative photon count
***
Golden Promise
Pwl2-YFP-2
Genotype
H
myc-HIPP43
Free-YFP
Pwl2-YFP
kDa
Free-YFP
Pwl2-YFP
kDa
In put
IP
40
27
20
α-GFP
α-myc
F
Putative interactor
PPIP10 (Thioredoxin)
PPIP9 (Catalase)
PPIP8 (Predicted protein)
PPIP7 (lipoxygenase)
PPIP6 (Cycophillin)
PPIP5 (Hypersensitive protein)
PPIP4 (HMA - domain protein)
PPIP3 (Peroxidase)
PPIP2 (Cysteine synthase)
PPIP1 (Lipase domain protein)
0 5 10 15 20
Peptide count Log2foldChange
I
SD/-L-T-H-A + X-α-gal
+ 3AT
HIPP43
pwl2-3
Pwl1
Pwl3
Pwl4
AVR-Pia
AVR-PikD
AVR-Mgk
G
SD/-L-T
SD/-L-T-H-A + X-α-gal
+ 3AT
DT7-T
DT7-T
Pwl2
-Lam
-53
Hv-HIPP43
1 10-1 10-2 10-3
1 10-1 10-2 10-3
J
Pwl2
Os-HIPP43
Ta-HIPP43
Ec-HIPP43
Si-HIPP43
1 10-1 10-2 10-3
1 10-1 10-2 10-3

Fig. 4. Pwl2 suppresses PAMP-induced ROS in transgenic barley lines and interacts with a host HIPP43.

(*A***)** Transgenic lines expressing Pwl2-YFP, control (free YFP) did not show growth defect compared to the background line, Golden Promise. (*B***)** ROS production in leaf discs collected from 4–week-old stable transgenic lines expressing Pwl2-YFP, control (free YFP) and Golden Promise induced by 1 uM chitin or flg22 (n > 8). Points represent mean; error bars represent SEM. (*C*) Dot plot shows cumulative ROS production over 60 min for Golden Promise control and Pwl2-YFP. The lower horizontal line shows the minimum value, and the upper horizontal line shows the maximum value, the middle line shows the mean value. Significance between groups of samples was performed using Unpaired Student's t-test. (*D*) Leaf drop infection on barley transgenic lines expressing free-YFP, Pwl2-YFP compared to infection on wild type Golden Promise 3-4 dpi. **(***E***)** The dot plot represents the number of rice blast disease lesions per 5 cm on Golden Promise, EV-YFP and Pwl2-YFP transgenic lines in three independent repetitions of the experiment. Unpaired Student's t-test was performed to determine significant differences. (*F***)** Putative Pwl2 interacting peptides were immunoprecipitated from protein extracted from 3-week-old stable Golden Promise transgenic lines expressing Pwl2-YFP or free cytoplasmic YFP using anti-GFP antibodies, and LC-MS/MS was performed to identify unique putatively interacting peptides. The scale 0-20 represents the Log2fold change in peptides when compared to the control. (*G***)** Pwl2 interacts with *Hv*HIPP43 in a yeast-two-hybrid assay. Simultaneous co-transformation of pGAD-Pwl2 (prey vector) and pGBK-HIPP43 (bait vector) and PGBKT7-53 and pGADT7-T (positive control) pGADTT7-T and pGBKT7-Lam (negative control) into Y2H gold strain resulted in the activation of four reporter genes and growth on high-stringency medium (−Ade, −Leu, –Trp, _His +X-α-gal and 3-amino-1,2,4-triazole). Co-transformation also activates the expression of *MEL1*, which results in the secretion of α–galactosidase and the hydrolysis of X-α-gal in the medium, turning the yeast colonies blue **(***H***)** Co-immunoprecipitation (co-IP) of Pwl2-YFP and Myc-HIPP43 in *N. benthamiana* leaves. C-terminal GFP tagged Pwl2 and C-terminal Myc-HIPP43 was cloned into the vector pGW514 and transformed into *Agrobacterium* strain *GV301* and co-infiltrated into *N. benthamiana* leaves and left to incubate for 48 h. Immunoprecipitates were obtained with anti-GFP or anti-Myc affinity matrix beads and probed with anti-GFP-peroxidase and anti-Myc-peroxidase (HRP-conjugated) antibodies. Total protein extracts were also probed with appropriate (HRP-conjugated) antibodies. (*I*) Yeast-two-hybrid analysis shows; upper panel, *Hv*HIPP43 interacts with *PWL* gene family products Pwl1, Pwl3, Pwl4 and variant *pwl2-3*. (*J*) Pwl2 binds to HIPP43 homologs from rice (*Os*HIPP43), wheat (*Taes*HIPP43), weeping love grass (*Ec*HIPP43), and foxtail millet (*Si*HIPP43).

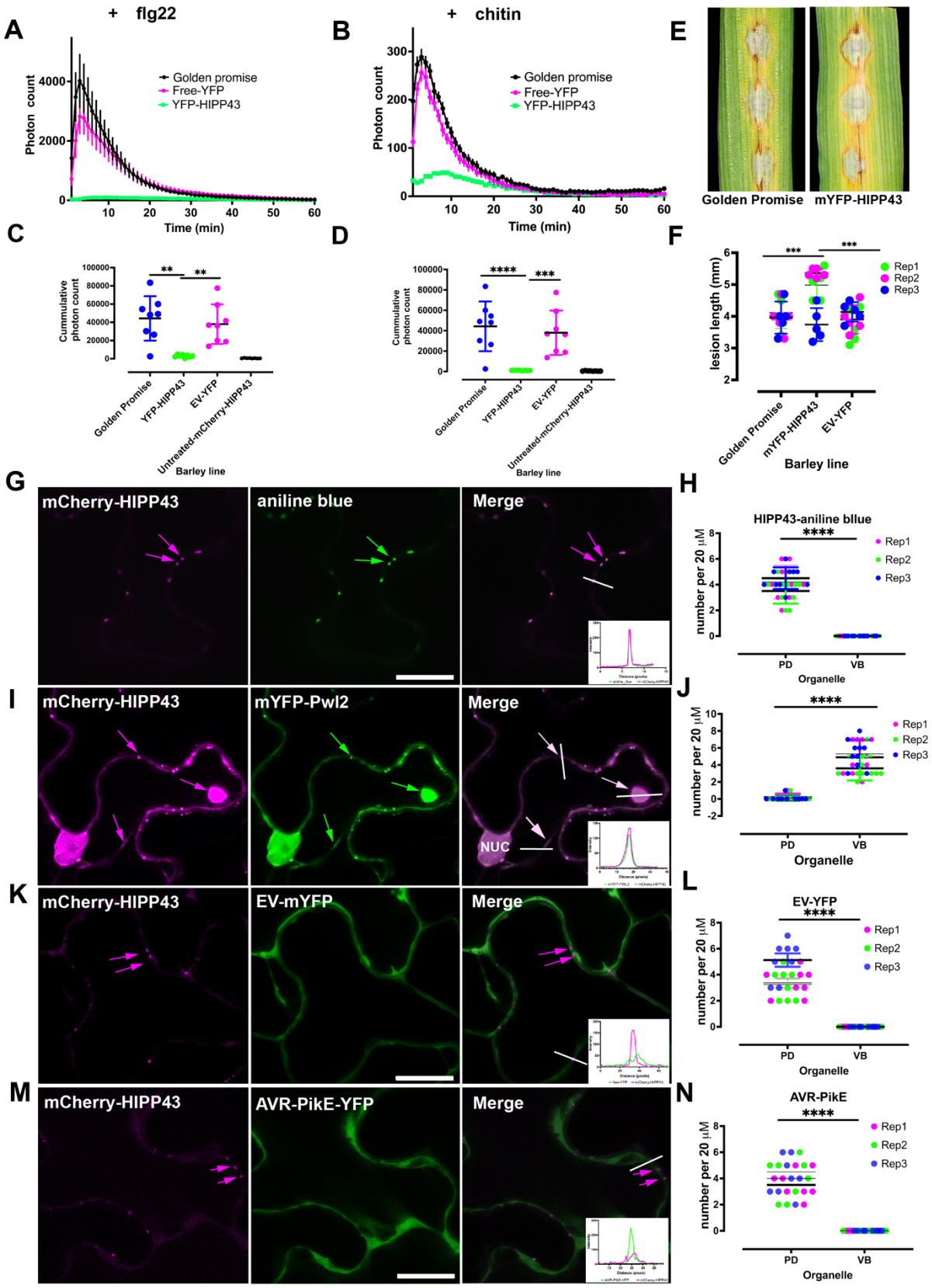
A
+ flg22
Photon count
Golden promise
Free-YFP
YFP-HIPP43
Time (min)
B
+ chitin
Photon count
Golden promise
Free-YFP
YFP-HIPP43
Time (min)
E
Golden Promise
mYFP-HIPP43
C
Cummulative photon count
Golden Promise
YFP-HIPP43
EV-YFP
Untreated-mCherry-HIPP43
Barley line
D
Cummulative photon count
Golden Promise
YFP-HIPP43
EV-YFP
Untreated-mCherry-HIPP43
Barley line
F
lesion length (mm)
Rep1
Rep2
Rep3
Golden Promise
mYFP-HIPP43
EV-YFP
Barley line
G
mCherry-HIPP43
aniline blue
Merge
H
HIPP43-aniline bllue
number per 20 μM
Rep1
Rep2
Rep3
PD
VB
Organelle
I
mCherry-HIPP43
mYFP-Pwl2
Merge
NUC
J
number per 20 μM
Rep1
Rep2
Rep3
PD
VB
Organelle
K
mCherry-HIPP43
EV-mYFP
Merge
L
EV-YFP
number per 20 μM
Rep1
Rep2
Rep3
PD
VB
Organelle
M
mCherry-HIPP43
AVR-PikE-YFP
Merge
N
AVR-PikE
number per 20 μM
Rep1
Rep2
Rep3
PD
VB
Organelle

807 **Fig. 5. HvHIPP43 suppresses PAMP-induced ROS in transgenic barley.**
808 **(***A-D***)** ROS production measured from leaf disks collected from 4–week-old stable transgenic
809 line expressing YFP-HIPP43 and Golden promise (control) in the absence and presence of 1
810 uM flg22 or 1 mg/ml Chitin (n > 8). For ROS assay, line graphs (upper panel) points represent
811 mean per time point and as cumulative ROS (*C*+*D*) production over 60 min, error bars
812 represent SEM. For dot plot graphs show the average cumulative photon count. The lower
813 horizontal line shows the minimum value, the upper horizontal line shows the maximum value,
814 the middle line shows the mean value. Significance between groups of samples was performed
815 using unpaired Student's t-test. ****P<0.0001, ***P<0.001, **P<0.01. (*E*) Leaf drop
816 infection on barley transgenic lines expressing YFP-HIPP43 compared to wild type Golden
817 Promise dpi. Conidial suspensions at 1 $\times 10^5$ mL^{-1} spores/mL from Guy11 were used to
818 inoculate 21-d-old seedlings of the blast-susceptible Golden Promise control and Golden
819 Promise expressing YFP-HIPP43. Disease symptoms were recorded after 5 dpi. (*F*) Dot plot
820 showing the average lesion size on barley lines infected with Guy11. The lower horizontal line
821 shows the minimum value, the upper horizontal line shows the maximum value, the middle
822 line shows the mean value. Significance between groups of samples was performed using
823 unpaired Student's t-test. ***P<0.001. **(***G*+*H***)** Micrographs and line scan graph showing
824 mCherry-HIPP43 localizing as small puncta on the plasma membrane when expressed in *N.*
825 *benthamiana.* Staining of callose using aniline blue overlaps with mCherry-HIPP43,
826 confirming mCherry-HIPP43 localises exclusively at the plasmodesmata (PD) localization and
827 is absent from vesicular bodies (VB). **(***I*+*J***)** Micrographs and line scan graph showing the
828 presence of YFP-Pwl2, alters m-Cherry-HIPP43 localisation, where it was observed to
829 translocate to the cytoplasm, cytoplasmic and vesicular structures **(***K*+*L***)** Micrographs and line
830 scan graph showing free-YFP fluorescence is observed in the cytoplasm and does not overlap
831 with mCherry-HIPP43 PD localization. **(***M*+*N*) Micrographs and line scan graph showing
832 mCherry-HIPP43 remains in the PD in the presence of cytoplasmically localised AVR-PikE**.**
833 Scale bars represent 20 µm**.** Significance between groups of samples was performed using
834 unpaired Student's t-test. ****P<0.0001.
835

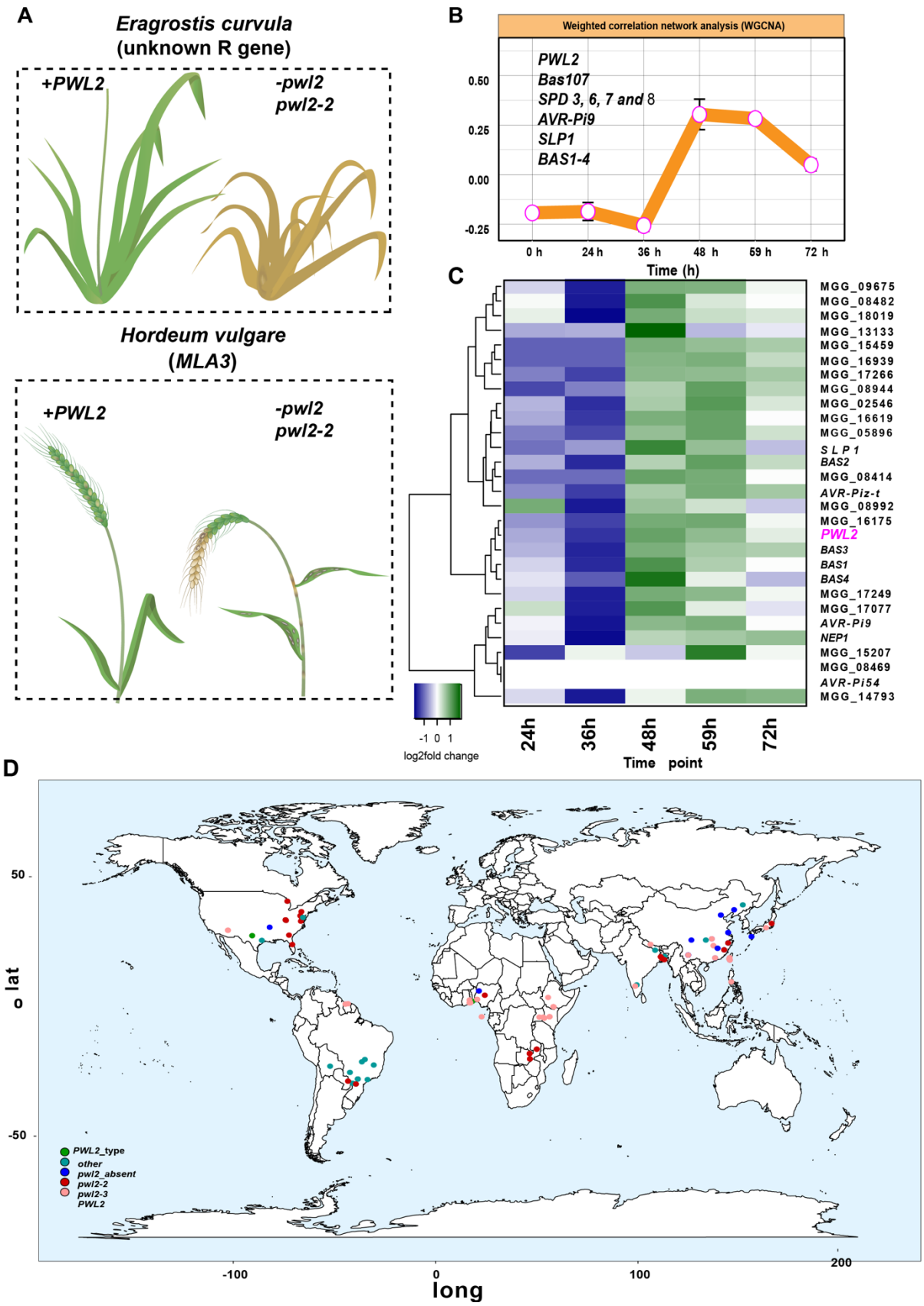
A
Eragrostis curvula
(unknown R gene)
+PWL2
-pwl2
pwl2-2
Hordeum vulgare
(MLA3)
+PWL2
-pwl2
pwl2-2
B
Weighted correlation network analysis (WGCNA)
PWL2
Bas107
SPD 3, 6, 7 and 8
AVR-Pi9
SLP1
BAS1-4
0.50
0.25
0.00
-0.25
0 h
24 h
36 h
48 h
59 h
72 h
Time (h)
C
MGG_09675
MGG_08482
MGG_18019
MGG_13133
MGG_15459
MGG_16939
MGG_17266
MGG_08944
MGG_02546
MGG_16619
MGG_05896
SLP1
BAS2
MGG_08414
AVR-Piz-t
MGG_08992
MGG_16175
PWL2
BAS3
BAS1
BAS4
MGG_17249
MGG_17077
AVR-Pi9
NEP1
MGG_15207
MGG_08469
AVR-Pi54
MGG_14793
-1 0 1
log2fold change
24h
36h
48h
59h
72h
Time point
D
50
-50
lat
PWL2_type
other
pwl2_absent
pwl2-2
pwl2-3
PWL2
-100
0
100
200
long

840 **Fig. S1. Pwl2 is co-expressed *in-planta* with other known effectors and is ubiquitous in**
841 **isolates of *M. oryzae* showing global distribution.**
842 (*A*) Illustration of how *PWL2* has been described as a host range determinant gene in weeping
843 lovegrass and barley. *M. oryzae* strain carrying *PWL2* produces incompatible reaction on
844 weeping lovegrass and cv. Baronesse (*Mla3*). (*B*) A susceptible rice line Moukoto, was infected
845 by a *M. oryzae strain* KE002 using leaf drop infection method and samples collected at 24, 36,
846 48, 59 and 72 hpi. RNA isolated from infected rice leaves were sequenced and the reads
847 normalized against *M. oryzae* mycelia KE002 RNA to determine differentially expressed
848 genes. A weighted gene co-expression network analysis grouped gene expression profile into
849 10 co-expression modules. The line graph (WGCNA) showing the representative eigengene
850 for module 4 in *PWL2* is co-expressed with other known effector protein encoding, *AVR-Pi9*,
851 *SLP1*, *BAS1-4* and a necrosis inducing effector *NEP1*. (*C)* Heatmap showing relative
852 expression levels (log2fold change) of *PWL2* and other know effectors during infection. (*D*)
853 Global distribution of Pwl2 alleles in *M. oryzae* isolates with publicly available genomes.
854 Tblastn was used determine presence of Pwl2 in *M. oryzae* genomes and *R* package *rworldmap*
855 v.1.3.4 used to create the map and occurrence of different alleles according to isolate point of
856 collection. *pwl2-2* mostly present in isolates from Asia while *pwl2-3* present in wheat blast
857 isolates from South America.

858

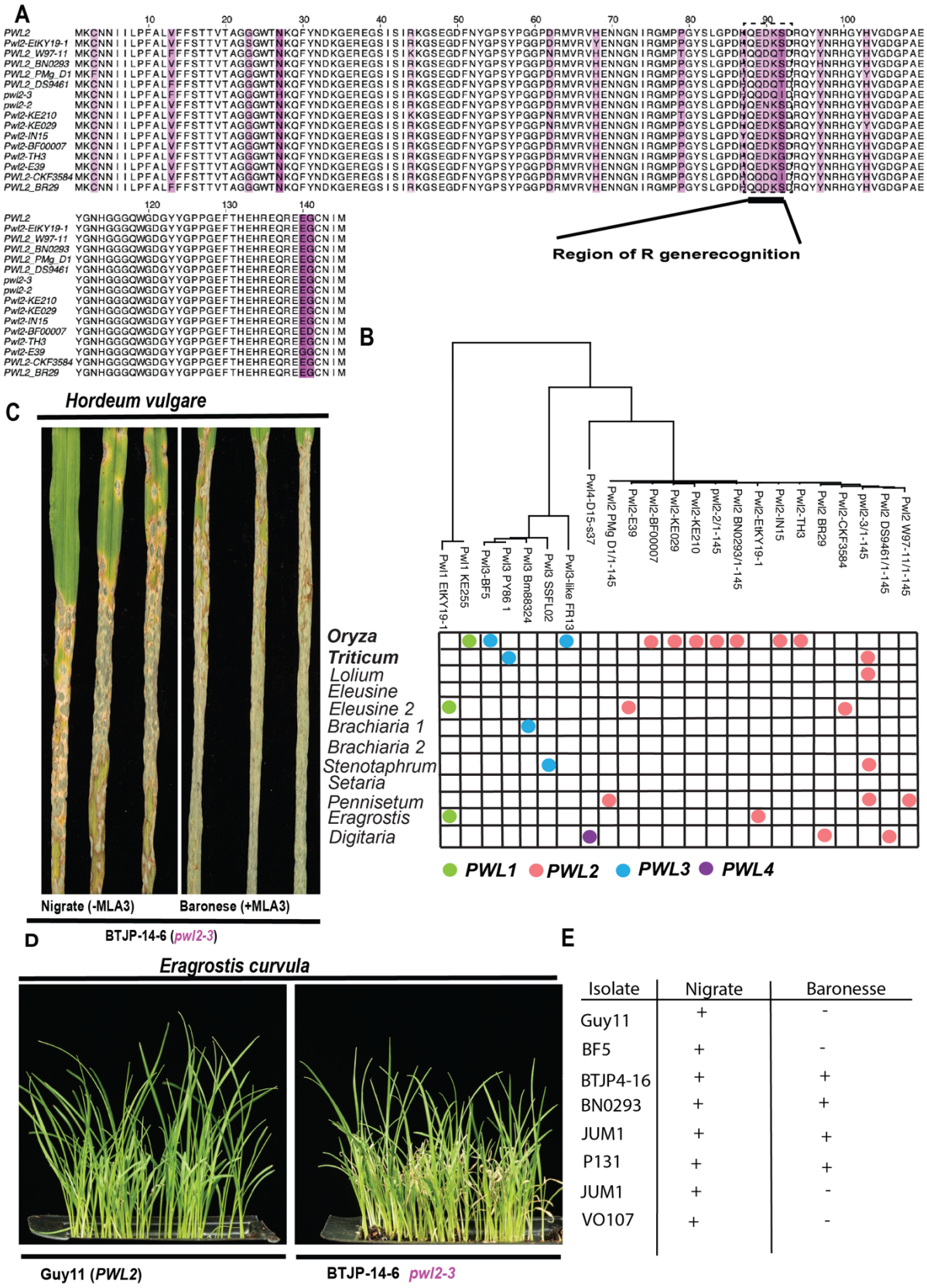

Isolate	Nigrate	Baronesse
Guy11	+	-
BF5	+	-
BTJP4-16	+	+
BN0293	+	+
JUM1	+	+
P131	+	+
JUM1	+	-
VO107	+	-

861 **Fig. S2. A variant of Pwl2, pwl2-3 is not recognized by Mla3 and cognate resistance**
862 **against Pwl2 in weeping lovegrass.**

863 (*A*) Multiple amino acid sequence alignment of Pwl2 protein and naturally occurring variants.
864 Alignment was carried using ClustalW (Jalview). (*B*) Neighbor-joining tree based on amino
865 acid sequence of variants encoded by *PWL* gene family. Tree IDs contains isolate name from
866 which the variant was identified, and each dot represent presence in each host-limited forms.
867 (*C* and *D*) Wheat blast isolate BTJP-14-6 carrying a *PWL2* variant, *pwl2-3* with Glu-89-Gln,
868 Lys-91-Gln and Ser-92-Ile substitutions was used for spray inoculation on barley accessions
869 cv. Golden promise (-*Mla3*) and cv. Baronesse (+*Mla3*) or (*D*) weeping lovegrass seedlings.
870 Disease symptoms on barley and weeping lovegrass were scored 5 and 7 days respectively,
871 post-infection. Observations were consistent in three independent infection replicates. (*E*)
872 Summary of disease reaction of isolates carrying variants of Pwl2 on Nigrate (-*Mla3*) and
873 Baronesse (+*Mla3*). Lesions on barley were scored 5 days post-infection.
874

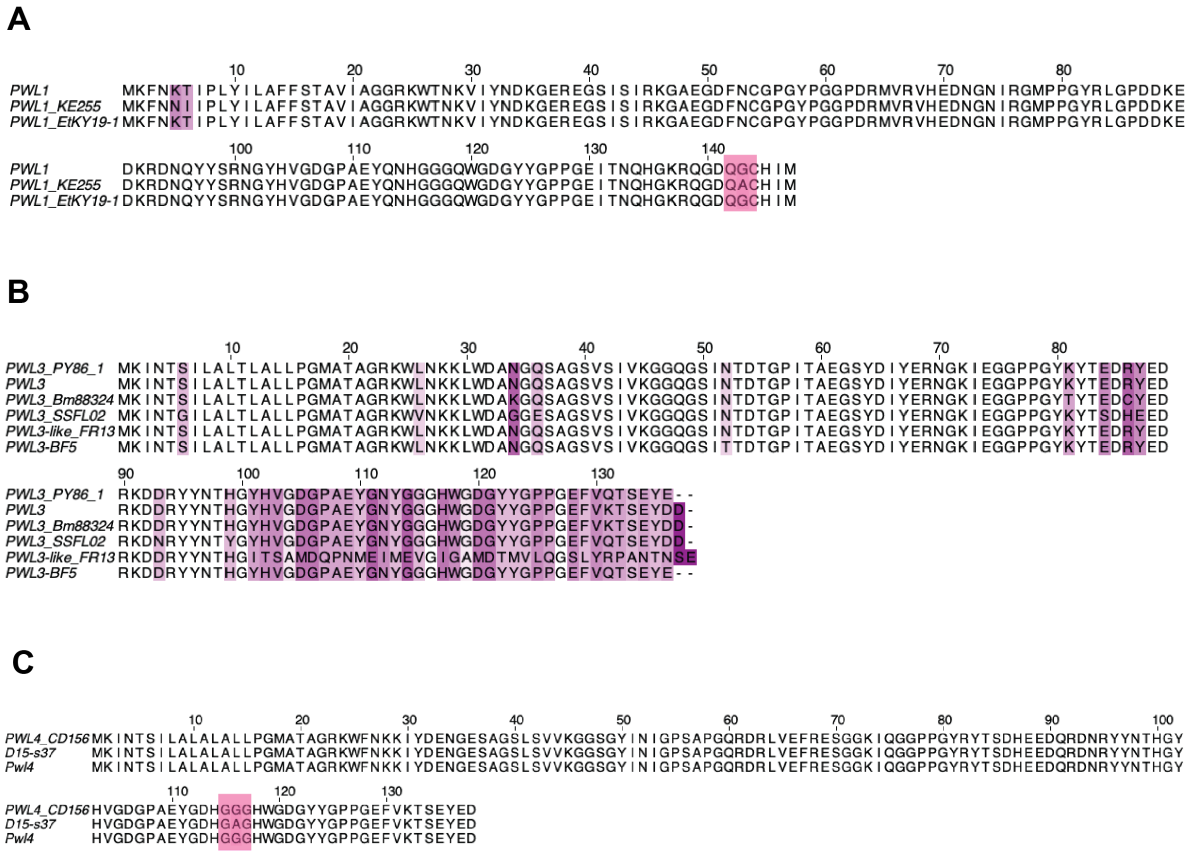

Fig. S3. *M. oryzae* isolates carry variants of Pwl1, Pwl3 and Pwl4 and copy number variation occurs in all rice blast genetic lineage groups.
Multiple amino acid sequence alignment of Pwl1 (*A*), Pwl3 (*B*) and Pwl4 (*C*) protein and naturally occurring variants. Alignment was carried using ClustalW (Jalview) regions or low conservation are shown in magenta.

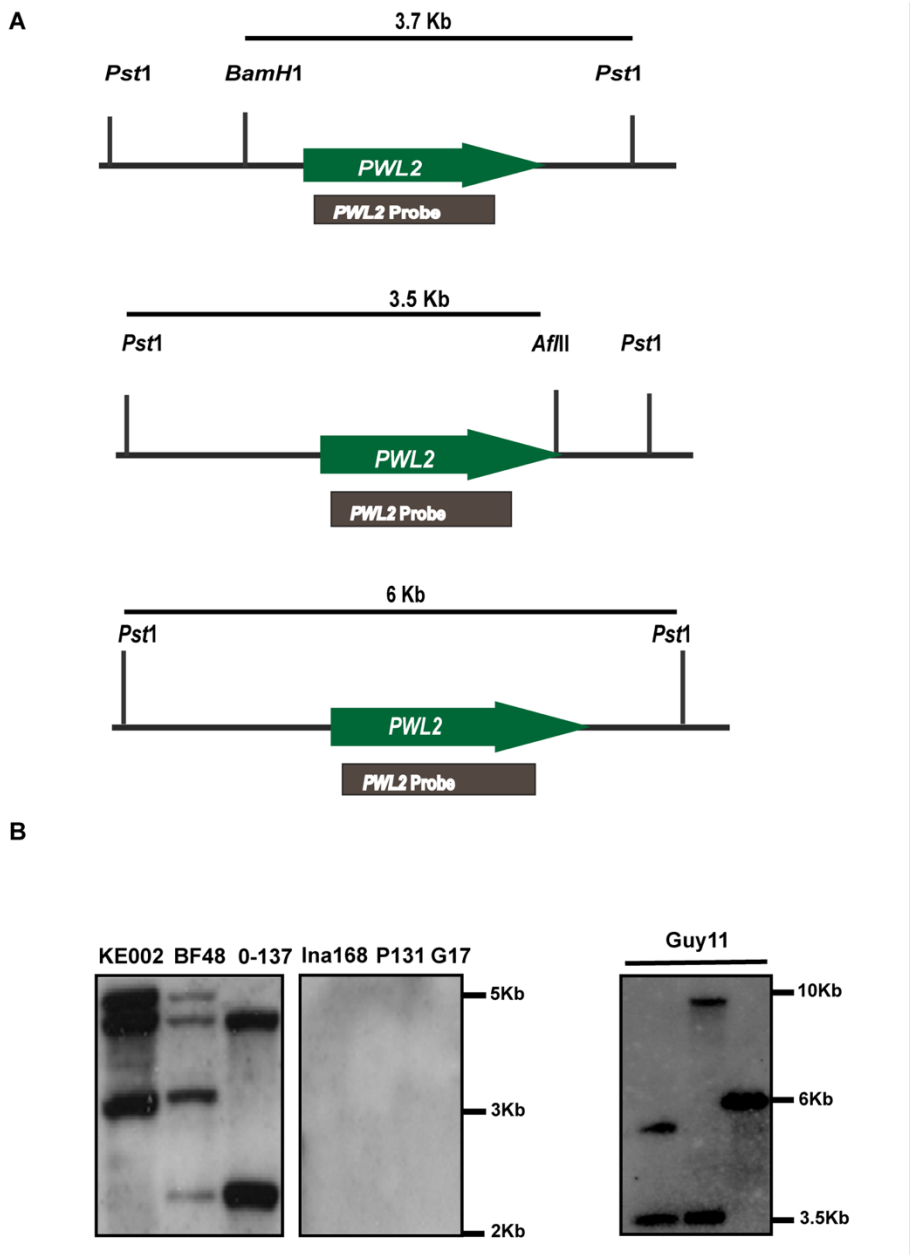

Fig. S4. Southern blot to determine copy number variation of *PWL2* in selected *M. oryzae* isolates.

(*A*) Genomic DNA was digested using different enzyme combination *Bam*H1/*Pst*1 and probed using the *PWL2* 438 bp probe. (*B*) The order of digested genomic DNA from different isolates is indicated on the lanes. Size estimates are from the *PWL2* loci annotated *M. oryzae* 70-15 genome. When Guy11 genomic DNA was digested using *Pst*1 and *Afl*II or single digested using *Afl*II, two bands were detected, a single digest using *Pst*1 only produce a single band.

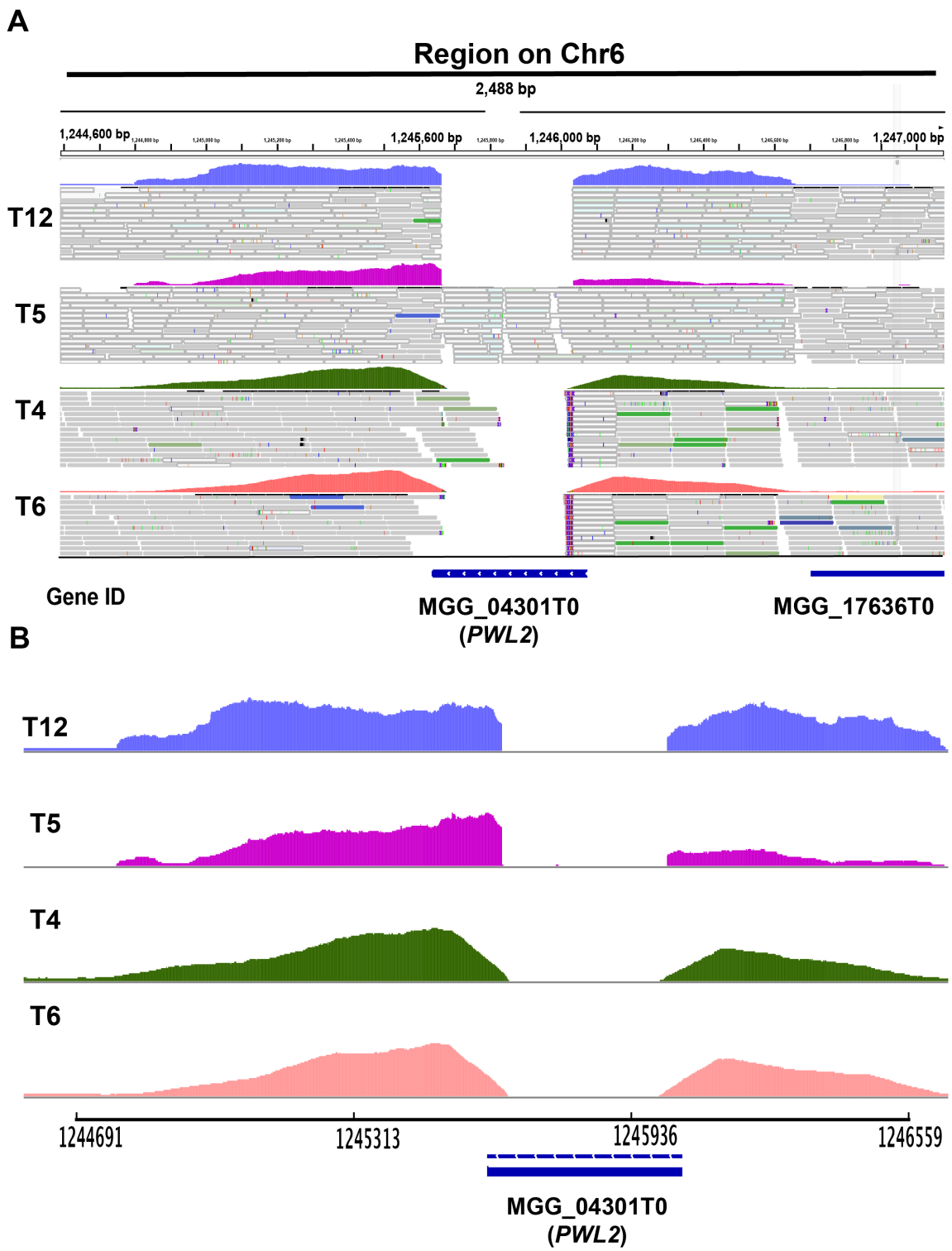

Fig. S5. Analysis of CRISPR-Cas9 mutants using Integrative Genomics Viewer (IGV). *(A)* Reads alignment display of *PWL2* locus on Chromosome 6 from four sequenced *pwl2* mutant strains, T12, T5, T4 and T6 (lower panel). No reads aligned at *PWL2* (MGG_04301T0) locus for T6 and T12 and partial alignment for T4 and T5. Read depth around *PWL2* locus is higher compared to the neighbouring gene MGG_17636T0 suggesting the *PWL2* locus occurs multiple times. Read coverage and locus length are indicated. (*B*) Sashimi plot showing depth of reads from T12, T5, T4 and T6 that aligned to the region surrounding *PWL2* locus.

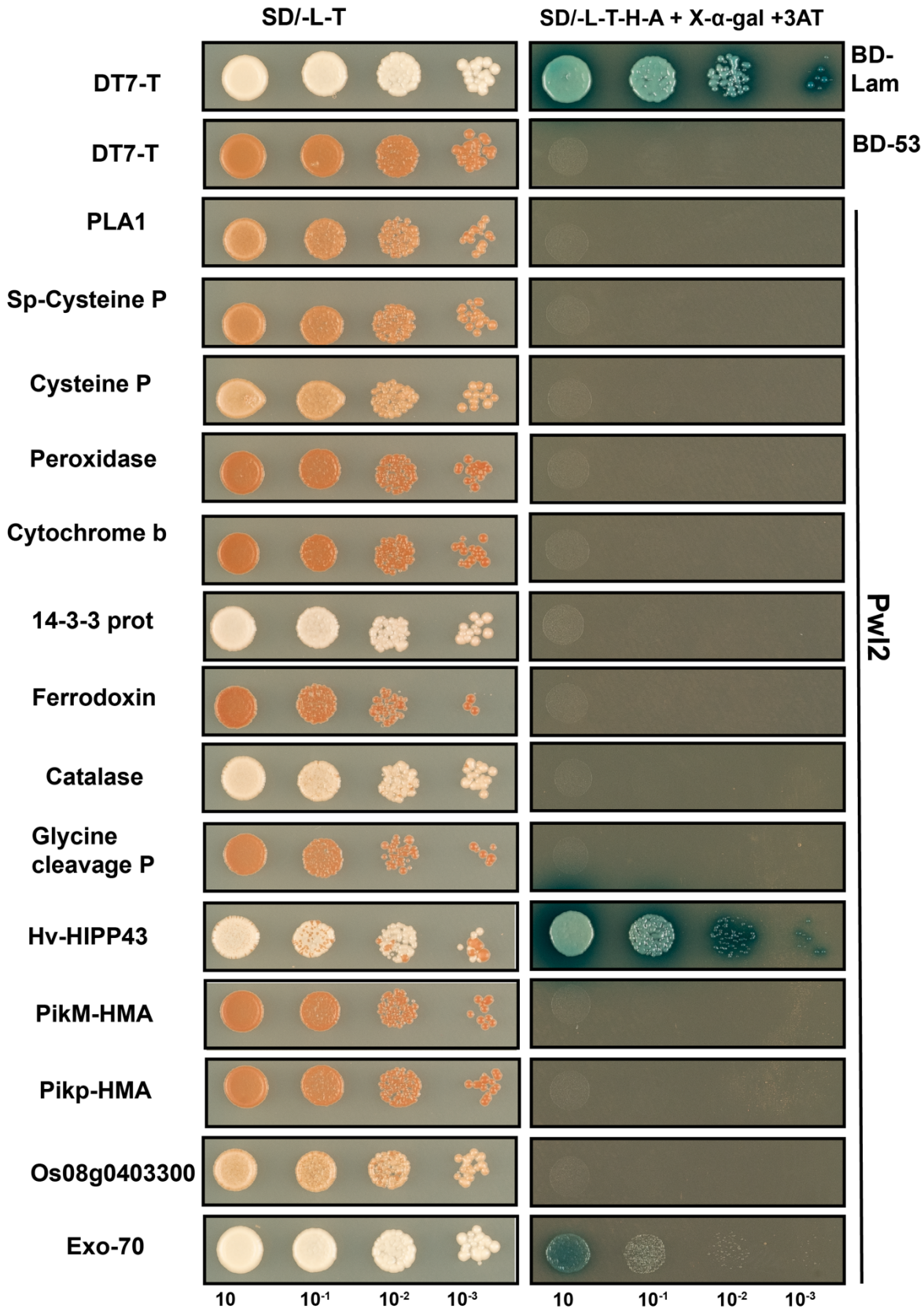
SD/-L-T
SD/-L-T-H-A + X-α-gal +3AT
DT7-T
DT7-T
PLA1
Sp-Cysteine P
Cysteine P
Peroxidase
Cytochrome b
14-3-3 prot
Ferrodoxin
Catalase
Glycine cleavage P
Hv-HIPP43
PikM-HMA
Pikp-HMA
Os08g0403300
Exo-70
BD-Lam
BD-53
Pwl2
10
10-1
10-2
10-3
10
10-1
10-2
10-3

906

907 **Fig. S6. Raw data results from Y2H assay with all other putative interactors from IP-MS.**
908 One-to-one yeast two-hybrid between Pwl2 and selected top candidates from IP-MS analysis,
909 Pwl2 and Putative Pwl2 Interacting Proteins (PPIPs). HMA integrated rice NLR Pikm-1 and
910 Pikp-1 were used as specificity controls. Simultaneous co-transformation of pGADT7-Pwl2
911 (prey vector) and pGBK-HIPP43 (bait vector) and PGBKT7-53 and pGADT7-T (positive
912 control) pGADTT7-T and pGBKT7-Lam (negative control) into Y2H gold strain resulted in
913 the activation of four reporter genes and growth on high-stringency medium (−Ade, −Leu, –
914 Trp, _His +X-α-gal and 3-amino-1,2,4-triazole). Co-transformation also activates the
915 expression of *MEL1*, which results in the secretion of α–galactosidase and the hydrolysis of X-
916 α-gal in the medium, turning the yeast colonies blue. HIPP43 exclusively bind Pwl2 in SD/-L-
917 T-H-A X-a-gal medium with 3AT added.
918

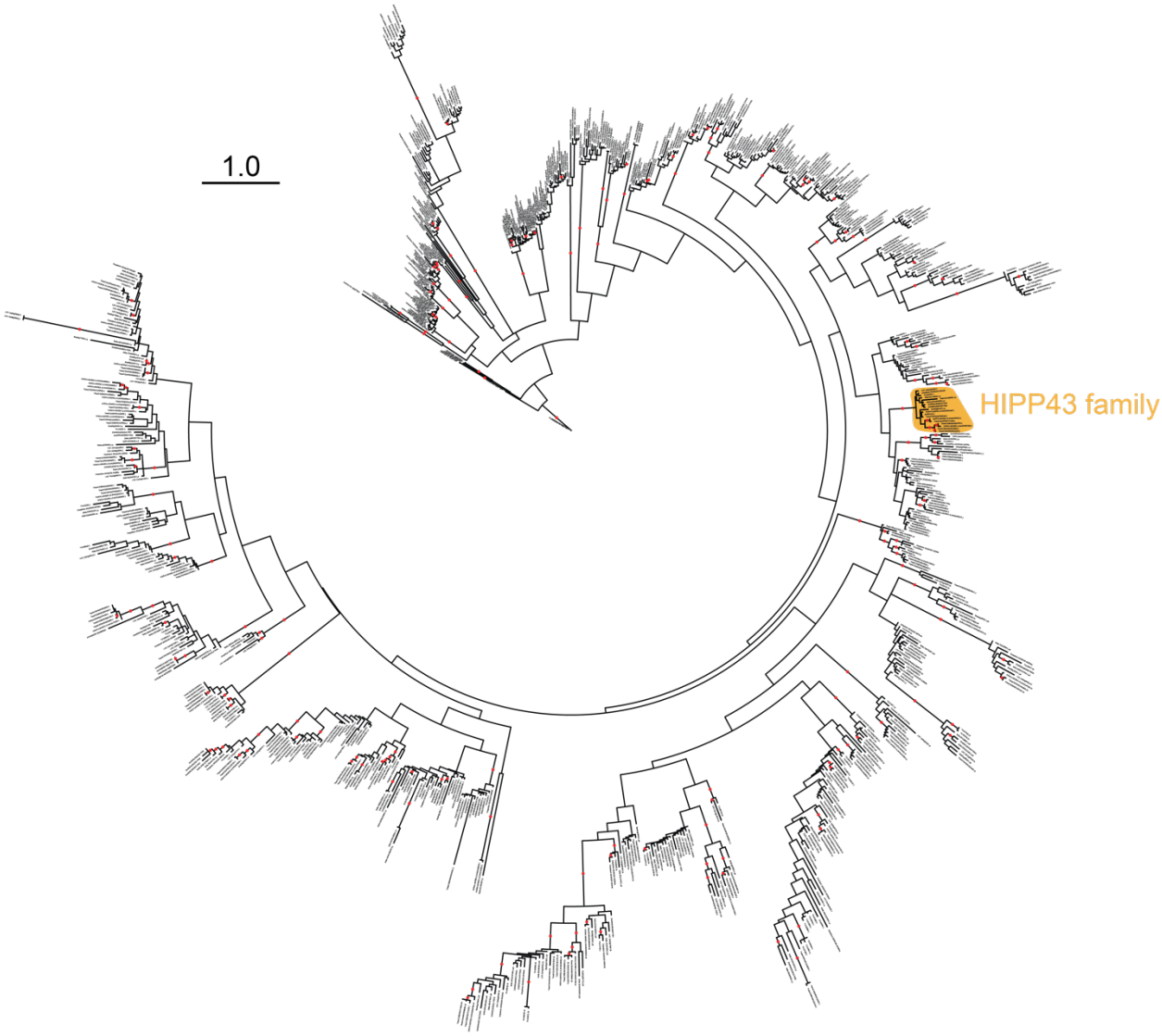

Fig. S7. Maximum likelihood phylogenetic tree of HMA domains from diverse grass species.

HMA domains were identified from proteins from the grass species *B. distachyon*, *H. vulgare*, *T. aestivum*, *O. sativa*, *Oropetium thomaeum*, *Sorghum bicolor*, *Setaria italica*, and *Zea mays*. Structure guided multiple sequence alignment was performed using MAFFT-DASH and phylogenetic analysis with RAxML. Scale bar indicates substitutions per site. Dots on branches indicate support of 80% or more based on 1,000 bootstraps. The HIPP43 family formed a distinct clade with bootstrap support of 98%.

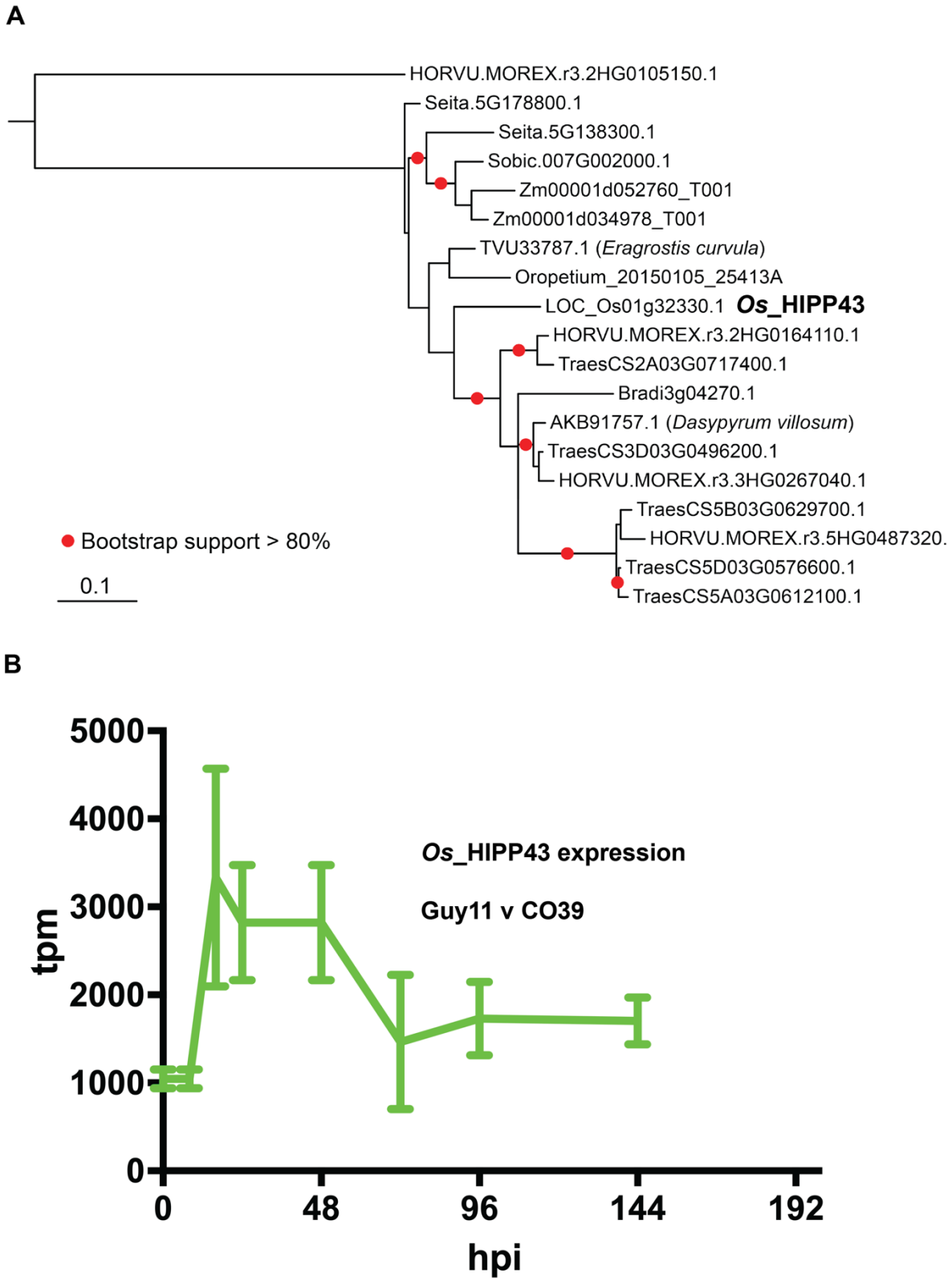

Fig. S8 Maximum likelihood phylogenetic tree for HIPP43 gene family.
(*A*) Full length coding sequence was identified for HIPP43 gene family members, aligned using MUSCLE translation alignment, and phylogenetic analysis with RAxML. Barley and wheat (i.e. *Triticeae* lineage) have three copies of HIPP43 per haploid genome. Dots on branches indicate support of 80% or more based on 1,000 bootstraps. (*B*) Expression at transcript level

937 of *Os*HIPP43 during infection of a susceptible rice cv. CO39 by Guy11. Hour post inoculation
938 is shown on the X –axis.
939
940
941
942
943
944

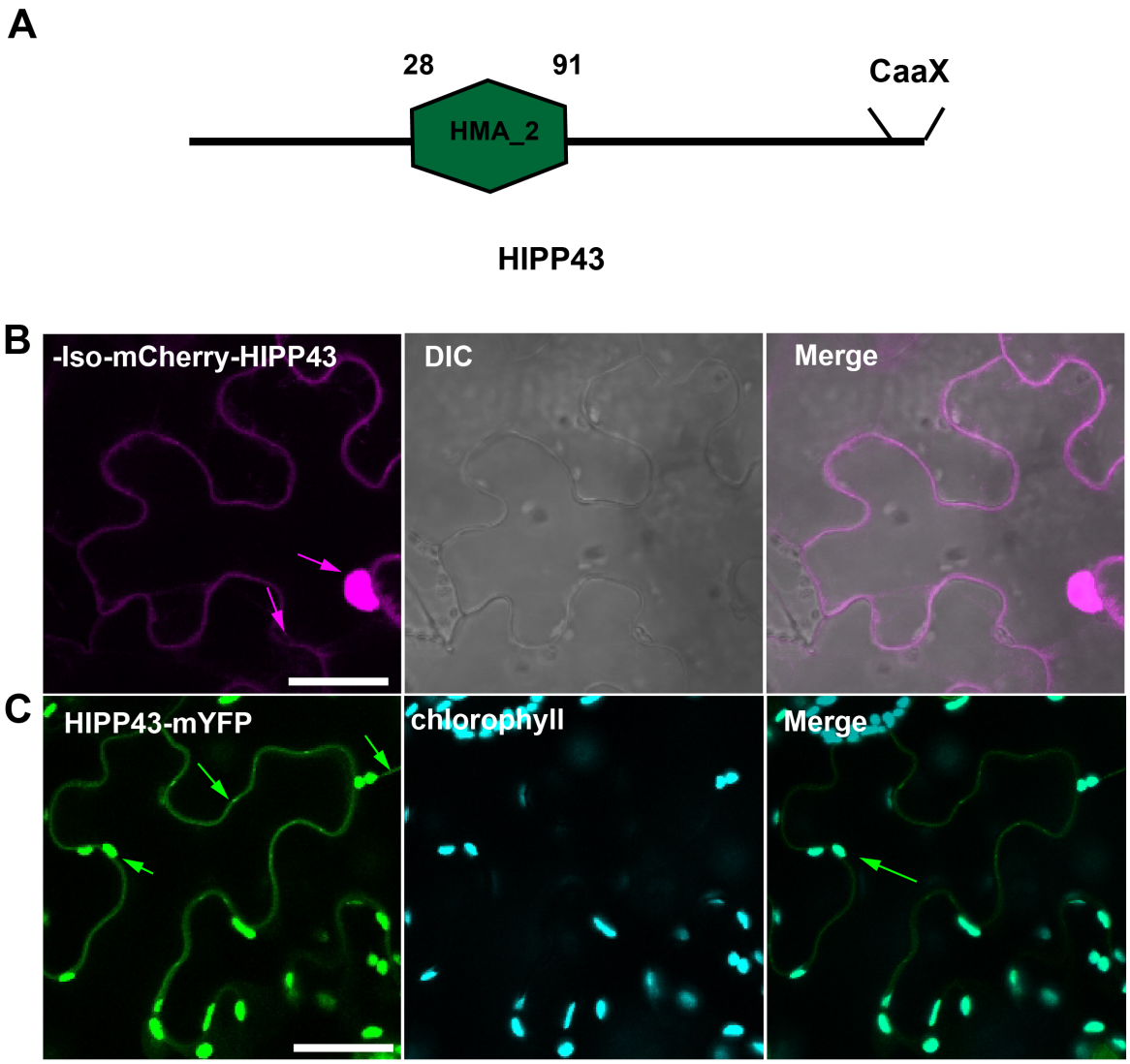

Fig. S9. HIPP43 isoprenylation motif is required for PD localisation.
(*A*) A schematic representation of domain structure of HIPP43 showing the HMA domain region and the isoprenylation motif at the C-terminus. (*B*+*C*) Micrographs showing localization of HIPP43 without the isoprenylation motif (-Iso-mCherry-HIPP43) and C-terminus tagged, HIPP43-YFP. (*B*) Deletion of the isoprenylation abolishes PD localisation but HIPP43 localises in the nucleus and partially in the plasma membrane and cytoplasm after 48h. **(***C***)** When HIPP43 was tagged at the C-terminus, localisation was observed in the plasma membrane, partially in the cytoplasm and PD, but predominantly in the chloroplast. Scale bars represent 20 µm.

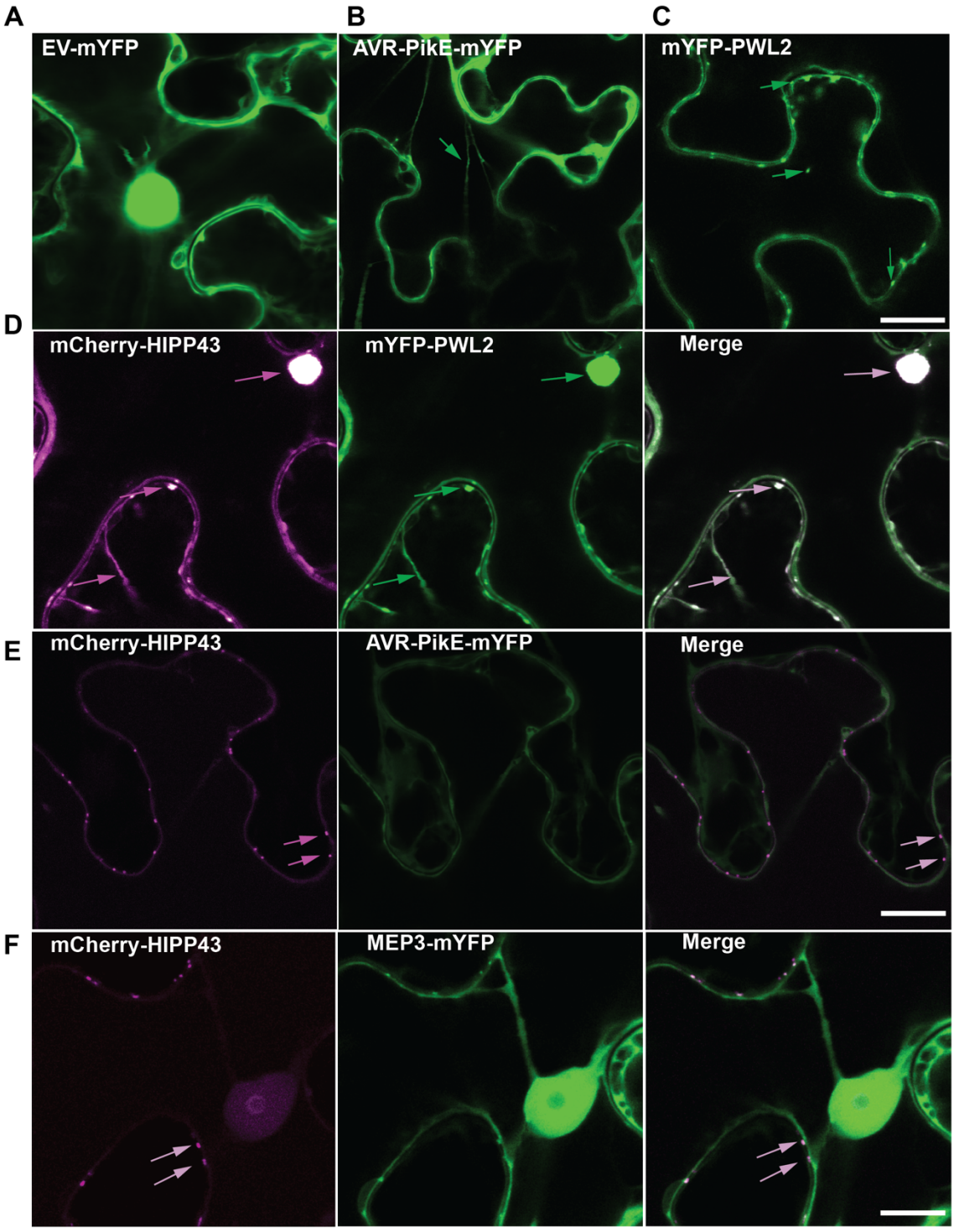

Fig. S10. Pwl2 promotes HIPP43 cytoplasmic localisation.
(*A-C*) Micrographs showing localization of free-YFP (A), AVR-PikE-YFP (B) and YFP-Pwl2 (C). Both free-YFP and AVR-PikE-YFP show localisation in the cytoplasm while YFP-Pwl2 showed localisation in cytoplasm and cytoplasmic mobile structures. (*D-F*) HIPP43 localisation in presence of AVR-PikE and Mep3 is unaffected but altered in the presence of Pwl2. **(***D***)** Micrographs showing that the presence of YFP-Pwl2, alters m-Cherry-HIPP43 localization, where it was observed to translocate to the cytoplasm and cytoplasmic vesicular structures. Arrows indicated cytoplasmic localization and cytoplasmic mobile bodies **(***E+F***)**

967 Micrographs showing HIPP43 is co-localisation with two different MAX-fold effectors AVR-
968 PikE and Mep3. mCherry-HIPP43 remains in the PD in the presence of cytoplasmically
969 localized AVR-PikE and Mep3. Arrows indicated PD. Scale bars represent 20 µm.
970
971

Table S1 Primers used in this study.

Primer	Sequence
PWL2ORF	ATGAAATGCAACAACATCATCCTCCC
PWL2ORR	ACATAATATTGCAGCCCTCTTCTCGC
PWL2f	GGTTCTTATTATGGTCCCGGGTGA
PWL2r	GGTTCTTATTATGGTCCCGGGTGA
PWL2848F	CGCGGTGGCGGCCGCTCTAGAGACCGGGCACGAACCCGGCAGGC
PWL2-R	CATAATATTGCAGCCCTCTT
PWL2_GFPF	GGGCTGCAATATTATGATGGTGAGCAAGGGCGAGGAGCTG
KOLFF	ACAACGCGGTGTAAAGATTCGGGT
KOLFR	GTCGTGACTGGGAAAACCCTGGCGAGACCAAAGCAAAAGGGAGGATGA
KORFF	TCCTGTGTGAAATTGTTATCCGCTGCGAGAAGAGGGCTGCAATATTA
PG514-myc-F	AACACGGGGGACTCTAGAGAACAAAAGTTGATCTCTGA
YFPPWL2-F	GACGAGCTGTACAAGGGTGGCGGGTGGACTAAC
PWL2-N-term-YFPR	GTTAGTCCACCCGCCACCCTTGTACAGCTCGTC
PWL2-R-p514	GAACGATCGGGGAAATTCGTTACATAATATTGCAGCCCT
HAPwl2F	AGAGAACACGGGGGACTCTAGAATGGGTGGCGGGTGGACTAAC
PG514-myc-F	AACACGGGGGACTCTAGAGAACAAAAGTTGATCTCTGA
myc-HIPP43-R	TCCAAGACGCCCATAAGGTCCTCTTCAGAAA
myc-HIPP43F	ATTTCTGAAGAGGACCTTATGGGCGTCTTGGA
HIPP43-NOS-R	ACGATCGGGGAAATTCGTCACATGATGGTGCAG
PG514-mCherry-F	AACACGGGGGACTCTAGAATGGTGAGCAAGGGC
mCherry-HIPP43F	GGACGAGCTGTACAAGATGGGCGTCTTGGA
mCherry-HIPP43R	TCCAAGACGCCCATCTTGTACAGCTCGTCC
KT7_HIPP34F	CATGGAGGCCGAATTCATGGGCGTCTTGGA
KT7_HIPP34R	GCAGGTCGACGGATCCTCACATGATGGTGCAG

981 **References**

982 1. J. D. Jones, J. L. Dangl, The plant immune system. *Nature* **444**, 323-329 (2006).

983 2. R. A. Wilson, N. J. Talbot, Under pressure: investigating the biology of plant infection
984 by *Magnaporthe oryzae*. *Nat Rev Microbiol* **7**, 185-195 (2009).

985 3. X. Yan *et al.*, The transcriptional landscape of plant infection by the rice blast fungus
986 *Magnaporthe oryzae* reveals distinct families of temporally co-regulated and
987 structurally conserved effectors. *The Plant Cell* **35**, 1360-1385 (2023).

988 4. E. Oliveira-Garcia, X. Yan, M. Oses-Ruiz, S. de Paula, N. J. Talbot, Effector-triggered
989 susceptibility by the rice blast fungus *Magnaporthe oryzae*. *New Phytologist* **n/a**
990 (2023).

991 5. Y. Sugihara *et al.*, Disentangling the complex gene interaction networks between rice
992 and the blast fungus identifies a new pathogen effector. *PLOS Biology* **21**, e3001945
993 (2023).

994 6. S. Cesari *et al.*, The Rice Resistance Protein Pair RGA4/RGA5 Recognizes the
995 *Magnaporthe oryzae* Effectors AVR-Pia and AVR1-CO39 by Direct Binding *The*
996 *Plant Cell* **25**, 1463-1481 (2013).

997 7. D. Ortiz *et al.*, Recognition of the *Magnaporthe oryzae* Effector AVR-Pia by the Decoy
998 Domain of the Rice NLR Immune Receptor RGA5. *The Plant Cell* **29**, 156-168 (2017).

999 8. I. Ashikawa *et al.*, Two Adjacent Nucleotide-Binding Site–Leucine-Rich Repeat Class
1000 Genes Are Required to Confer Pikm-Specific Rice Blast Resistance. *Genetics* **180**,
1001 2267-2276 (2008).

1002 9. H. Kanzaki *et al.*, Arms race co-evolution of *Magnaporthe oryzae* AVR-Pik and rice
1003 Pik genes driven by their physical interactions. *The Plant Journal* **72**, 894-907 (2012).

1004 10. K. de Guillen *et al.*, Structure Analysis Uncovers a Highly Diverse but Structurally
1005 Conserved Effector Family in Phytopathogenic Fungi. *PLoS Pathog* **11**, e1005228
1006 (2015).

1007 11. A. Maqbool *et al.*, Structural basis of pathogen recognition by an integrated HMA
1008 domain in a plant NLR immune receptor. *eLife* **4**, e08709 (2015).

1009 12. X. Zhang *et al.*, A positive-charged patch and stabilized hydrophobic core are essential
1010 for avirulence function of AvrPib in the rice blast fungus. *The Plant Journal* **96**, 133-
1011 146 (2018).

1012 13. J. A. Sweigard *et al.*, Identification, cloning, and characterization of PWL2, a gene for
1013 host species specificity in the rice blast fungus. *Plant Cell* **7**, 1221-1233 (1995).

1014 14. H. J. Brabham *et al.*, Barley MLA3 recognizes the host-specificity effector Pwl2 from
1015 *Magnaporthe oryzae*. *The Plant Cell* 10.1093/plcell/koad266, koad266 (2023).

1016 15. Rafał Zdrzałek *et al.*, Bioengineering a plant NLR immune receptor with a robust
1017 recognition interface towards a conserved fungal pathogen effector. *bioRxiv* (2024).

1018 16. N. Suzuki, Y. Yamaguchi, N. Koizumi, H. Sano, Functional characterization of a heavy
1019 metal binding protein CdI19 from *Arabidopsis*. *The Plant Journal* **32**, 165-173 (2002).

1020 17. P. E. Dykema *et al.*, A new class of proteins capable of binding transition metals. *Plant*
1021 *Molecular Biology* **41**, 139-150 (1999).

1022 18. W. Gao, S. Xiao, H.-Y. Li, S.-W. Tsao, M.-L. Chye, *Arabidopsis thaliana* acyl-CoA-
1023 binding protein ACBP2 interacts with heavy-metal-binding farnesylated protein AtFP6.
1024 *New Phytologist* **181**, 89-102 (2009).

1025 19. M. Hála, V. Žárský, Protein Prenylation in Plant Stress Responses.
1026 http://dx.doi.org/10.3390/molecules24213906.

1027 20. S. Fukuoka *et al.*, Loss of function of a proline-containing protein confers durable
1028 disease resistance in rice. *Science* **325**, 998-1001 (2009).

1029 21. K. Oikawa *et al.*, The blast pathogen effector AVR-Pik binds and stabilizes rice heavy
1030 metal-associated (HMA) proteins to co-opt their function in immunity. *bioRxiv*
1031 10.1101/2020.12.01.406389, 2020.2012.2001.406389 (2020).

1032 22. A. R. Bentham *et al.*, A single amino acid polymorphism in a conserved effector of the
1033 multihost blast fungus pathogen expands host-target binding spectrum. *PLoS Pathog*
1034 **17**, e1009957 (2021).

1035 23. M. C. Giraldo *et al.*, Two distinct secretion systems facilitate tissue invasion by the rice
1036 blast fungus *Magnaporthe oryzae*. *Nat Commun* **4**, 1996 (2013).

1037 24. E. Oliveira-Garcia *et al.*, Clathrin-mediated endocytosis facilitates the internalization
1038 of *Magnaporthe oryzae* effectors into rice cells. *The Plant Cell* **35**, 2527-2551 (2023).

1039 25. P. Kankanala, K. Czymmek, B. Valent, Roles for rice membrane dynamics and
1040 plasmodesmata during biotrophic invasion by the blast fungus. *Plant Cell* **19**, 706-724
1041 (2007).

1042 26. Kang S.C., Sweigard J.A., V. B, The PWL host specificity gene family in the blast
1043 fungus *Magnaporthe grisea*. *Molecular Plant-Microbe Interactions* **8**, 939-948 (1995).

1044 27. N. J. Talbot, On the trail of a cereal killer: Exploring the biology of *Magnaporthe*
1045 *grisea*. *Annu Rev Microbiol* **57**, 177-202 (2003).

1046 28. S. H. Ou, Pathogen Variability and Host-Resistance in Rice Blast Disease. *Annu Rev*
1047 *Phytopathol* **18**, 167-187 (1980).

1048 29. C. D. Cruz, B. Valent, Wheat blast disease: danger on the move. *Trop Plant Pathol* **42**,
1049 210-222 (2017).

1050 30. Y. Inoue *et al.*, Evolution of the wheat blast fungus through functional losses in a host
1051 specificity determinant. *Science* **357**, 80-83 (2017).

1052 31. S. Asuke *et al.*, Evolution of an Eleusine-Specific Subgroup of *Pyricularia oryzae*
1053 Through a Gain of an Avirulence Gene. *Mol Plant Microbe Interact* **33**, 153-165
1054 (2020).

1055 32. S. M. Latorre *et al.*, Genomic surveillance uncovers a pandemic clonal lineage of the
1056 wheat blast fungus. *PLOS Biology* **21**, e3002052 (2023).

1057 33. A. J. Foster *et al.*, CRISPR-Cas9 ribonucleoprotein-mediated co-editing and
1058 counterselection in the rice blast fungus. *Scientific Reports* **8**, 14355 (2018).

1059 34. A. Sánchez-Vallet, J. R. Mesters, B. P. H. J. Thomma, The battle for chitin recognition
1060 in plant-microbe interactions. *FEMS Microbiology Reviews* **39**, 171-183 (2015).

1061 35. T. Shimizu *et al.*, Two LysM receptor molecules, CEBiP and OsCERK1, cooperatively
1062 regulate chitin elicitor signaling in rice. *The Plant Journal* **64**, 204-214 (2010).

1063 36. R. Mostafa *et al.*, Recombination of standing variation in a multi-hybrid swarm drove
1064 adaptive radiation in a fungal pathogen and gave rise to two pandemic plant diseases.
1065 *bioRxiv* 10.1101/2021.11.24.469688, 2021.2011.2024.469688 (2021).

1066 37. D. Pereira, U. Oggenfuss, B. A. McDonald, D. Croll, Population genomics of
1067 transposable element activation in the highly repressive genome of an agricultural
1068 pathogen. *Microb Genom* **7** (2021).

1069 38. J. H. R. Maidment *et al.*, Multiple variants of the fungal effector AVR-Pik bind the
1070 HMA domain of the rice protein OsHIPP19, providing a foundation to engineer plant
1071 defense. *Journal of Biological Chemistry* **296** (2021).

1072 39. N. Mukhi *et al.*, Perception of structurally distinct effectors by the integrated WRKY
1073 domain of a plant immune receptor. *Proc Natl Acad Sci U S A* **118** (2021).

1074 40. W. Zschiesche *et al.*, The zinc-binding nuclear protein HIPP3 acts as an upstream
1075 regulator of the salicylate-dependent plant immunity pathway and of flowering time in
1076 *Arabidopsis thaliana*. *New Phytologist* **207**, 1084-1096 (2015).

1077 41. O. Barth, S. Vogt, R. Uhlemann, W. Zschiesche, K. Humbeck, Stress induced and
1078 nuclear localized HIPP26 from *Arabidopsis thaliana* interacts via its heavy metal
1079 associated domain with the drought stress related zinc finger transcription factor
1080 ATHB29. *Plant Molecular Biology* **69**, 213-226 (2009).

1081 42. H. Zhang *et al.*, Characterization of the Heavy-Metal-Associated Isoprenylated Plant
1082 Protein (HIPP) Gene Family from *Triticeae* Species. *Int J Mol Sci* **21** (2020).

1083 43. Z. K. Barr, T. Werner, J. Tilsner, Heavy Metal-Associated Isoprenylated Plant Proteins
1084 (HIPPs) at Plasmodesmata: Exploring the Link between Localization and Function.
1085 http://dx.doi.org/10.3390/plants12163015.

1086 44. G. H. Cowan *et al.*, Potato Mop-Top Virus Co-Opts the Stress Sensor HIPP26 for Long-
1087 Distance Movement. *Plant Physiol* **176**, 2052-2070 (2018).

1088 45. J. B. de Abreu-Neto, A. C. Turchetto-Zolet, L. F. V. de Oliveira, M. H. Bodanese
1089 Zanettini, M. Margis-Pinheiro, Heavy metal-associated isoprenylated plant protein
1090 (HIPP): characterization of a family of proteins exclusive to plants. *The FEBS Journal*
1091 **280**, 1604-1616 (2013).

1092 46. Z. Wang *et al.*, Isoprenylation modification is required for HIPP1-mediated powdery
1093 mildew resistance in wheat. *Plant Cell Environ* **46**, 288-305 (2023).

1094 47. Q. M. Imran *et al.*, Nitric Oxide Responsive Heavy Metal-Associated Gene AtHMAD1
1095 Contributes to Development and Disease Resistance in *Arabidopsis thaliana*. *Front*
1096 *Plant Sci* **7**, 1712 (2016).

1097 48. Z. S. Radakovic *et al.*, Arabidopsis HIPP27 is a host susceptibility gene for the beet
1098 cyst nematode *Heterodera schachtii*. *Mol Plant Pathol* **19**, 1917-1928 (2018).

1099 49. T. Guo *et al.*, Arabidopsis HIPP proteins regulate endoplasmic reticulum-associated
1100 degradation of CKX proteins and cytokinin responses. *Mol Plant* **14**, 1918-1934
1101 (2021).

1102 50. R. O'Lexy *et al.*, Exposure to heavy metal stress triggers changes in plasmodesmatal
1103 permeability via deposition and breakdown of callose. *Journal of Experimental Botany*
1104 **69**, 3715-3728 (2018).

1105 51. Z. Wang *et al.*, Isoprenylation modification is required for HIPP1-mediated powdery
1106 mildew resistance in wheat. *Plant, Cell & Environment* **46**, 288-305 (2023).

1107 52. N. J. Talbot, D. J. Ebbole, J. E. Hamer, Identification and characterization of MPG1, a
1108 gene involved in pathogenicity from the rice blast fungus *Magnaporthe grisea*. *Plant*
1109 *Cell* **5**, 1575-1590 (1993).

1110 53. B. Valent, L. Farrall, F. G. Chumley, *Magnaporthe grisea* Genes for Pathogenicity and
1111 Virulence Identified through a Series of Backcrosses. *Genetics* **127**, 87-101 (1991).

1112 54. H. Sakai *et al.*, Rice Annotation Project Database (RAP-DB): an integrative and
1113 interactive database for rice genomics. *Plant Cell Physiol* **54**, e6 (2013).

1114 55. R. A. Dean *et al.*, The genome sequence of the rice blast fungus *Magnaporthe grisea*.
1115 *Nature* **434**, 980-986 (2005).

1116 56. D. Kim *et al.*, TopHat2: accurate alignment of transcriptomes in the presence of
1117 insertions, deletions and gene fusions. *Genome Biol* **14**, R36 (2013).

1118 57. S. Anders, W. Huber, Differential expression analysis for sequence count data. *Genome*
1119 *Biol* **11**, R106 (2010).

1120 58. E. Southern, Southern blotting. *Nat Protoc* **1**, 518-525 (2006).

1121 59. F. Sambrook J, E.F., and Maniatis, T Molecular Cloning - a laboratory manual, second
1122 edition. . *Cold Spring Harbour Laboratory press* (1989).

1123 60. H. Li, R. Durbin, Fast and accurate short read alignment with Burrows-Wheeler
1124 transform. *Bioinformatics* **25**, 1754-1760 (2009).

1125 61. M. Holsters *et al.*, The functional organization of the nopaline *A. tumefaciens* plasmid
1126 pTiC58. *Plasmid* **3**, 212-230 (1980).

1127 62. G. Hensel, C. Kastner, S. Oleszczuk, J. Riechen, J. Kumlehn, Agrobacterium-mediated
1128 gene transfer to cereal crop plants: current protocols for barley, wheat, triticale, and
1129 maize. *Int J Plant Genomics* **2009**, 835608 (2009).

1130 63. B. WN, Burnette WN. "Western Blotting": electrophoretic transfer of proteins from
1131 sodium dodecyl sulfate-polyacrylamide gels to unmodified nitrocellulose and
1132 radiographic detection with antibody and radioiodinated protein. *Analytical*
1133 *Biochemistry* **112**, 195 - 203 (1981).

1134 64. H. Li *et al.*, Pathogen protein modularity enables elaborate mimicry of a host
1135 phosphatase. *Cell* **186**, 3196-3207.e3117 (2023).

1136